이학박사학위논문

동아시아의 지면변화가 기후모의에 미치는 영향

The Impacts of Land Surface Changes on Climate Simulation over East Asia

2015 년 2 월

서울대학교 대학원

지구환경과학부

조 미 현

Abstract

The Impacts of Land Surface Changes on Climate Simulation over East Asia

Mee-Hyun Cho

School of Earth and Environmental Sciences

The Graduate School

Seoul National University

Although on a global scale, the radiative forcing estimates of landscape alteration appear to be small (about -0.2±0.2 Wm^{-2}), in East Asia where the landscape changes have been intensive, the impact of land use and land cover change (LULCC) is comparable to those of greenhouse gases and sea surface temperatures. In order to better understand the historical climate changes, impact of land cover change on climate has been widely

investigated. But in East Asia, there are few studies to assess effects of cropland management within existing croplands and impacts of land cover change and its accompanying dust aerosol. In this study, it will be proposed regional climate responses to land surface changes after harvest in the North China Plain of a double cropping region and the impacts of land cover generated by dynamic vegetation model on East Asian climate.

In the relation to the cropland management, this study reports the impacts of land use alterations from harvesting practices on the regional surface climate over the North China Plain. Observational analysis and modeling results showed that the land surface was warmer and drier after harvest. The bare soil surface after harvest in June has biophysical impacts on the surface climate that were mediated by decreasing evapotranspiration and latent heat flux effects, which increased surface temperatures and decreased surface humidity. Under two Representative Concentration

Pathways (RCP) scenarios, land conversion induced additional warming in addition to greenhouse gases induced global warming.

In the relation to the land cover generated by dynamic vegetation model, it was investigated the impacts of land cover change, as simulated by a dynamic vegetation model, on the summertime climatology over Asia. The climate model used in this study has systematic biases of underestimated rainfall around Korea and overestimation over the South China Sea. When coupled to a dynamic vegetation model, the resulting change in land cover is accompanied by an additional direct radiative effect over dust-producing regions. The direct radiative effect of the additional dust contributes to increasing the rainfall biases, while the land surface physical processes are related to local temperature biases such as warm biases over North China. In time-slice runs for future climate, as the dust loading changes, anomalous anticyclonic flows are simulated over South China Sea, resulting in reduced rainfall over the South China Sea and more

rainfall toward around Korea and South China. In contrast with the rainfall changes, the influence of land cover change and the associated dust radiative effects are very small for future projection of temperature, which is dominated by atmospheric CO2 increase. The results suggest that the land cover simulated by a dynamic vegetation model can affect, and be affected by, model systematic biases on regional scales over dust emission source regions such as Asia. In particular, analysis of the radiative effects of dust changes associated with land cover change is important in order to understand future changes of regional precipitation in global warming.

Key words: Land use and land cover change, East Asia, Climate Simulation, North China Plain, Dust radiative effect, Earth System Model

Student Number: 2003-30139

CONTENTS

Table Legends

Figure Legends

Chapter 1. Introduction

1.1 Motivations and scientific objectives

With increases in greenhouse gases (GHGs) concentrations and aerosol loading, the alteration of the Earth's surface due to changes in landscape is regarded as a significant human-induced change. Anthropogenic land surface change is one of the few climate forcings with still unknown sign of their climate response. IPCC Fourth Assessment Report (AR4) gave a best estimation of radiative foring (RF) relative to 1750 due to land use related surface albedo -0.2±0.2 Wm^{-2}[Solomon et al., 2007]. Although on a global scale, the RF estimates of landscape alteration appear to be small, in regions where the landscape changes have been intensive, the impact of land-use

land-cover change (LULCC) is comparable to those of GHGs and sea surface temperatures (SSTs) [Pielke et al., 2011 and references therein; De Noblet-Ducoudré et al., 2012]. In order to better understand the historical climate changes, impact of agriculture on climate has been widely investigated [Bonan, 2001; Cooley et al., 2005; Douglas et al., 2006; Lobell et al., 2006; Nair et al., 2007; Roy et al., 2007; Lee et al., 2009; Osborne et al., 2009; Takata et al., 2009; Ge, 2010; Yamashima et al., 2011; Ho et al., 2012; Kueppers and Snyder, 2012].

Land surface property changes have effects on the atmosphere through physical processes (such as changes in surface roughness, albedo and evapotranspiration), and can induce additional indirect impacts when coupled with aerosol processes as well. For example, changes in surface emissions of mineral dust that are caused by changes in bare soil fraction will have a radiative effect in the atmosphere.

Furthermore, the land surface properties are important in seasonal climate simulations because of their known impact on the local circulation [Pielke and Avissar, 1990] and on the East Asian monsoon [Suh and Lee, 2004; Kang et al., 2005; Kang and Hong, 2008; Lee et al., 2011] and on the Indian monsoon [Douglas et al., 2006; Lee et al., 2009; Bayer et al., 2012]. Lee et al. [2011] proposed that a replacement of vegetation with bare soil would cause an associated decrease in latent heat during the summer, which could weaken East Asian monsoon circulation. This decrease in latent heat flux over land could weaken differential heating between land and ocean which is one of the fundamental driving mechanisms of the monsoon. The subsequent weakened land-sea temperature gradient alters regional circulation patterns and monsoon conditions. In south China, it is reported that cultivation induced land use change has altered seasonal hydro-climate. According to Yamashima et al. [2011],

historical changes in land use from forest to cultivated land have resulted in a decrease in the monsoon rainfall over the Indian subcontinent and southeastern China and has provoked an associated weakening of the Asian summer monsoon circulation.

In Asia, the land surface changes by human activities have been an important research subject because the land surface changes have been intensive historically over there. Over 50% of the world's population is concentrated in Asia, and the region has experienced a large LULCC due to agricultural development [Takata et al., 2009]. Particularly, China has become the most heavily populated and rapidly developing country in the world during the last few decades. Agriculture in China feeds about 22% of the global population, using only 7% of the world's arable lands. Rice, wheat, and maize are the main crops, together accounting for 54% of the total sown area and 89% of the grain yield in 2007 [Piao et al., 2010].

In this study, it will be proposed the impact of land surface changes on East Asian climate. Above previous studies discuss the importance of land use and land cover changes on regional climate. Although impact of land cover change on climate has been widely investigated in order to better understand the historical climate changes, there are few studies to assess effects of cropland management within existing agricultural lands over East Asia. And there are a few studies about impacts of land cover change and its accompanying dust aerosol on East Asian climate. Through this study, we can investigate the physical influence of land cover conditions and associated aerosol loading on the rainfall and surface temperature over East Asia.

1.2 Organization of thesis

This study is organized with two major sections and corresponding subsections. Detailed descriptions are same as follows. Section 2 is dealt with an impact of land surface changes after harvest in the North China Plain under present and possible future. Section 2.2 describes the model datasets and the experimental configuration used in this study; Section 2.3 introduces the observed results for land use change (LUC) effects over the double-cropping region in the NCP; Section 2.4 analyzes the climate model results under present and possible future climate conditions.

In the Section 3, it is described the impact of land cover generated by dynamic vegetation model on East Asian climate. Section 3.2 briefly describes the global circulation model used in this study, the experimental design, and the data. The results of the study are given in section 3.3. The impact of land cover distribution and radiative effect of dust under present and possible future climate are

all provided in this section. The paper is closed in section 4 describing summary and discussions.

Chapter 2. Regional climate response to land surface changes after harvest in the North China Plain under present and possible future climate conditions

2.1 Backgrounds

Cultivation-related land use change made a considerable impact on aspects of climate [Takata et al., 2009; Pielke et al, 2011]. Interannual variations in land surface properties associated with crop growth and development have been found to have a significant impact on near-surface fluxes and climate [Osborne et al., 2009]. Ho et al. [2012] reported that the harvested land areas show a warmer surface temperature than the surrounding regions. Ge [2010] also

showed a similar result in the study involving the southern Great Plains of the US after harvest. It is well known that the harvesting of crops dramatically alters the energy, momentum, and water fluxes between the atmosphere and its underlying surface [Cooley et al., 2005; Pielke et al. 2007], and that responses of surface climate by the land use changes are more conspicuous at regional scales [Nair et al., 2007; Ray et al., 2006; Roy et al, 2007; Pielke et al. 2011].

It is well known that expansion of agriculture into natural ecosystems can have important climatic consequences, but changes occurring within existing croplands also have the potential to affect local climate [Lobell et al., 2006]. Although a number of studies such as Feddema et al. [2005], Pitman and Narisma [2005], Pitman et al. [2011] and Lawrence et al. [2012] have assessed the impact of landscape changes on regional surface temperature and precipitation under possible future climate conditions, few studies to assess that of

land use changes within existing cropland for future has been performed. Based on those previous studies, it is investigated the biophysical impacts of land use change under different GHG induced climate conditions. And to simplify the problem it is assumed that there is no land cover change related with agricultural expansion over the North China Plain (hereafter NCP), in other words, that the future cropland management is assumed to be identical with present. To project possible future climate, it is considered two Representative Concentration Pathways (RCP) scenarios 2.6 and 8.5. It must be noted that the biogeochemical impact of harvest on local climate was not taken into account as the atmosphere-only simulations were performed in this study.

In this study, the NCP region is focusing of huge croplands with flat and relatively homogeneous agricultural practices and a high cropland density above 70%, as shown in satellite data [Liu et al.,

2005]. In summer, winds blow from the ocean to the land transporting moisture to the East Asian continent and the NCP affects the Asian monsoon system as the NCP is located at the upstream of the south-westerly flow. Hence there arises a vital need to understand the changes driven by land-use management in land cover over the NCP. The purpose of this study is assessing the response of local climate induced from landscape changes after harvest, and so it is confined the analysis period to June, the month after harvesting.

2.2 Model Experimental Design

In this study, it was performed atmosphere-only simulations using the atmosphere version of the Hadley Center Global Environmental Model (HadGEM2-A, version 2) that had been

developed by the UK Met Office [Collins et al., 2011]. The horizontal grid interval was 1.25° × 1.875° in the latitude-longitude directions, and 38 vertical layers were used with the top of atmosphere over 39 km in height. The relatively coarse horizontal resolution enabled us to minimize the use of computational resources, and therefore more ensemble members were allowed in this study. The land surface scheme in HadGEM2-A is a tiled version of the Met Office Surface Exchange Scheme (MOSES) 2, which represents heterogeneous surface properties [Cox et al., 1999; Essery and Clark, 2003]. A grid box represents a mixture of five vegetation or plant-functional types (PFTs), which include broadleaf tree, needleleaf tree, temperate C_3 grass, tropical C_4 grass, and shrubs, and four non-vegetated surface types, which include urban, inland water, bare soil, and ice. Surface fluxes and temperatures were calculated separately for each surface type and were aggregated according to each tile's fractional coverage

before being passed to the atmospheric model [Lawrence and Slingo, 2004].

To investigate the impact of harvest on the regional climate over the NCP under present climate and RCP scenarios, six sets of experiments were conducted: two sets for present-day conditions (CTR and HAV; 1984–2005), two sets for the RCP 2.6 scenario (CTR26 and HAV26; 2071–2090), and two sets for the RCP 8.5 scenario (CTR85 and HAV85; 2071–2090) (Table 2.1). The abbreviations CTR and HAV represent the control and harvest experiments, respectively. All experiments were performed using the uncoupled atmosphere model. The simulations HAV, HAV26, and HAV85 shared the same set-up parameters as CTR, CTR26, and CTR85, except that their fractional vegetation covers varied on a monthly basis. In order to reduce uncertainty in the model results, it is designed five ensemble members for each set of experiment, which sums to total 30 runs,

with different starting and spin-up times for the integrations so that each one have the same analysis periods: periods from 1984 to 2005 and from 2071 to 2090 were analyzed for present and possible future, respectively. The initial conditions for the present run were chosen from historical runs of the HadGEM2-AO [Baek et al., 2013].

Present-day simulations were carried out using both time-varying forcings for GHG concentrations and aerosols and natural forcings as specified by the CMIP5 (phase five of the Coupled Model Intercomparison Project) for the AR5 (the Fifth Assessment Report). Details of the boundary conditions used for the atmosphere-only experiment in this study were similar to those of coupled historical simulations by Baek et al. [2013] and Jones et al. [2011], except for the sea surface temperatures (SSTs), sea ice, and fractional vegetation cover. The model integration used a prescribed dataset of observed Global sea-Ice and Sea Surface Temperature (GISST) dataset (Rayner

et al., 1996). All forcings were identical in both the CTR and HAV, except for the fractional vegetation cover.

For the fractional vegetation cover, the International Geosphere–Biosphere Programme (IGBP) climatology was used, which is based on HYDE3 (History Database of the Global Environment) and Loveland et al. [2000] (Figure 2.1b); this experiment is referred to here as "the control run" (CTR). The leaf area index (LAI) has a seasonal cycle affected by the air temperature evolution. As the combination of the constant C_3 fraction (Figure 2.1b) and the seasonally varying LAI were used for CTR, the experiment can be safely assumed to be an equivalent single cropping experiment. While a single predefined temporal behavior for fractional vegetation cover may be adequate for natural vegetation, such an estimate may be inappropriate to use for agricultural crops because these areas may differ drastically depending upon the agricultural practices [Nair et al., 2007]. Over the

NCP, wheat is harvested in May and maize is then planted again at the end of June almost simultaneously as appeared in the Moderate Resolution Imaging Spectroradiometer (MODIS) LAI observation in Figure 2.2. The fraction of C_3 was then swapped for the fraction of soil in June after wheat harvest (C_3), and the fraction of C_4 (i.e., maize) was increased from July to September (Figure 2.1a). Because the post-harvest residue is burned, left on the soil, or plowed into the soil [Cooley et al., 2005], this type of change for the land fraction seems reasonable. The area where this type of land cover fraction was applied is shown in Figure 2.1c, and it corresponds to the double-cropping area in Liu et al. [2005]. In this study, the monthly varying land cover fraction experiment is called "HAV."

To understand the impacts of harvest under the RCP scenarios, additional experiments were performed using the RCP 2.6 and RCP 8.5 scenarios, in addition to the present-day experiments. For the

prescribed SST and sea ice data, it is used projected changes for SST and sea ice from the RCP 2.6 and 8.5 scenarios, with respect to the present-day run from the HadGEM2-AO results from Baek et al. [2013]. The increments were added onto the SST and sea ice conditions of the present-day runs. Forcings of GHGs and aerosols were applied, as specified by the CMIP5 RCP scenario. Each of these experiment sets also had five ensemble members. As it is assumed that there is no land cover change related with agricultural expansion over the NCP, the fractional vegetation covers used in the possible future runs were the same as the present ones.

Table 2.1. Configurations of the experiments.

Acronyms for the experiments	Descriptions of the experiments	Analysis period
CTR	Control run in present-day	1984–2005
HAV	Harvest run in present-day	1984–2005
CTR26	Control run under RCP 2.6 scenario	2071–2090
HAV26	Harvest run under RCP 2.6 scenario	2071–2090
CTR85	Control run under RCP 8.5 scenario	2071–2090
HAV85	Harvest run under RCP 8.5 scenario	2071–2090

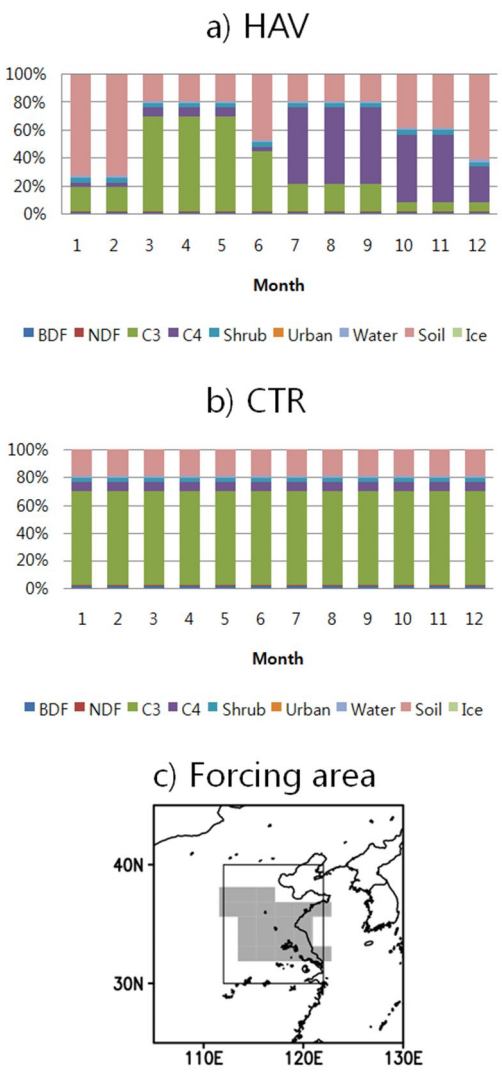

Figure 2.1. Monthly fractional vegetation cover over the North China Plain during the (a) harvest (HAV) and (b) control (CTR) simulations used in this study. (c) The analyzed domain used in the HadGEM2-Atmosphere model for the harvest experiment is shown by the gray box over the North China Plain.

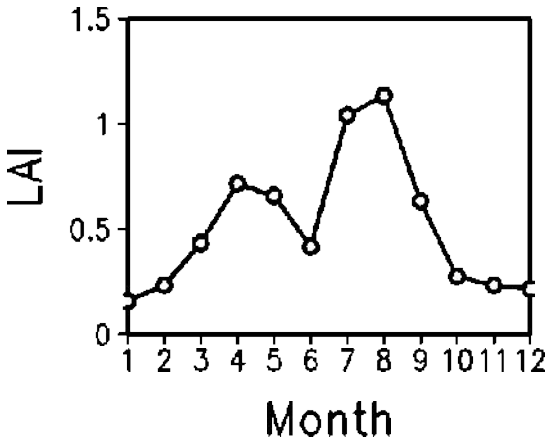

Figure 2.2. Monthly variation of leaf area index (LAI) from MODIS (Moderate Resolution Imaging Spectroradiometer) averaged over the harvest region for the period 2004–2008.

2.3 Observational analysis

LAI values, which is used as an indicator of biological land surface properties, shows a similar evolution with air temperature over the seasonal cycle for natural vegetation. For example, the seasonal cycle displayed one peak per year in the mid-latitude region,

but this did not appear in multi-cropping regions. Instead, the MODIS LAI at the double-cropping stations over the NCP showed two peaks over the seasonal cycle (Figure 2.2). Because there is wheat during the spring and maize during the summer, the LAI values for June were much lower than for May. These agriculture-induced land surface seasonal changes are readily apparent in Figure 2.2. The MODIS LAI data were used to classify the harvest and near single-cropping stations. The number of harvesting and near single-cropping stations analyzed was twelve.

The climatic impacts caused by the harvesting of winter wheat were evaluated from station observations collected during the period from 1996 to 2005. Specifically, monthly temperature and relative humidity data were analyzed. The observations showed that the averaged differences of monthly surface air temperatures and relative humidity between June and May were 0.8°C warmer and 5.7% drier

in the harvest area than in areas near the single-cropping region (Table 2.2, Figure 2.3). These results were similar to those of Ho et al. [2012], which reveal that the difference between the mean daily maximum temperatures averaged over the harvest region and the near single-cropping region peaks at 1.27°C in June over the NCP. The northeastern region of the domain showed significant increases of relative humidity with strong increase of surface air temperature. The increases can be mainly attributed to the moisture convergence by the enhanced southerly flow component in June relative to that in May in this region. Moreover, surface air temperature increase is thought to contribute partly to the decrease of the relative humidity by increasing saturation vapor pressure from the Clausius-Clapeyron equation. In addition to the changes observed in the surface air temperatures, the increments in surface temperatures using satellite

data were even more enhanced. More explanations will be given in 2.4.2.

Table 2.2. Average surface atmospheric variables and the difference between harvesting and surrounding vegetated stations from 1996 to 2005.

Stations	Temperature [°C]	Relative humidity [%]
vegetated	4.1	4.9
harvesting	4.9	-0.7
harvesting - vegetated	0.8	-5.6

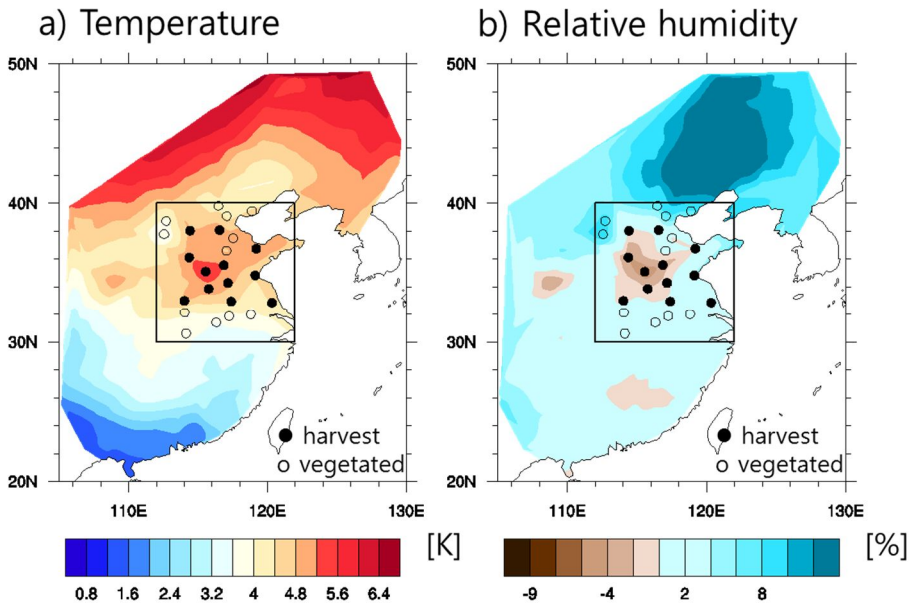

Figure 2.3. Post-harvest changes in (a) air temperatures (°C) and (b) relative humidity (%) measured at observation stations over China (1996–2005). The changes represent differences in values between the June harvesting period and the May crop covered period. The black circles represent harvesting stations. The rectangular box within each panel denotes the analysis domain used in this study.

2.4 Model Results

2.4.1 Model Performance

A measurement of climate model performance over East Asia (100–145°E, 20–50°N) was carried out to understand the effects of harvest on present-day climate simulations. In order to calculate the skill of the model's performance for each run, it is followed the method described by Reichler and Kim [2008] and Kim and Reichler [2011]. The performance of HAV and CTR was evaluated by this index with CMIP3 (phase three of the Coupled Model Intercomparison Project) models. In determining the model performance indices, it is first calculated for each model and variable a normalized error variance E^2 by squaring the grid-point

differences between simulated (interpolated to the observational grid) and observed climate, normalizing on a grid-point basis with the observed interannual variance, and averaging globally.

$$E^2 = \sum_{n=1}^{N} w_n \left(\frac{\overline{s_n} - \overline{o_n}}{\sigma_{n,o}} \right)^2$$

Where $\overline{s_n}$ is the simulated climatology for grid point (n), $\overline{o_n}$ the corresponding observed climatology, w_n the latitudinally varying area weights, and $\sigma_{n,o}$ the interannual variance from the validating observations, respectively. The normalization with the interannual variance helped to homogenize errors from different variables. In order to ensure that different climate variables received similar weights when combining their errors, it is next scaled E^2 by the average error found in a reference ensemble of models. The reference ensemble was the present-day CMIP3 experiment.

$$I_r^2 = \frac{E_r^2}{\overline{E_g^2}^m}$$

The validation data are presented in Table 2.3. Fourteen climate variables (Table 2.3) were selected for analysis over East Asia (Figure 2.4). Here, smaller index values are indicative of better model performance. In Figure 2.4, the HAV index values for most of variables were smaller than those of the CTR, except for precipitation and meridional winds. These results reflect slightly improved simulation skills over East Asia. In particular, the HAV performed better at simulating upward shortwave radiation at the surface and near surface temperatures. These data imply that the monthly varying conditions of land use fraction can contribute to the improvements of climate simulations over East Asia.

Table 2.3. Climate variables and corresponding validation data.

Variable	Acronym	Validation Data
Total cloudiness	CLT	CERES, ISCCP
Precipitation	PR	CMAP, GPCP
Surface downwelling longwave flux in air	RLDS	BSRN, CERES, GEBA, ISCCP
Surface upward shortwave flux	RSUS	BSRN, CERES, GEBA, ISCCP
TOA outgoing longwave flux	RLUT	CERES, ERBE, ISCCP, NOAA
Surface downwelling shortwave flux in air	RSDS	BSRN, CERES, GEBA, ISCCP
TOA outgoing shortwave flux	RSUT	CERES, ERBE, ISCCP
200 hPa air temperature	T200	ERA-40
2m air temperature	TAS	ERA-40
200hPa zonal wind	U200	ERA-40

850hPa zonal wind	U850	ERA-40
200hPa meridional wind	V200	ERA-40
850hPa meridional wind	V850	ERA-40
500hPa geopotential height	Z500	ERA-40

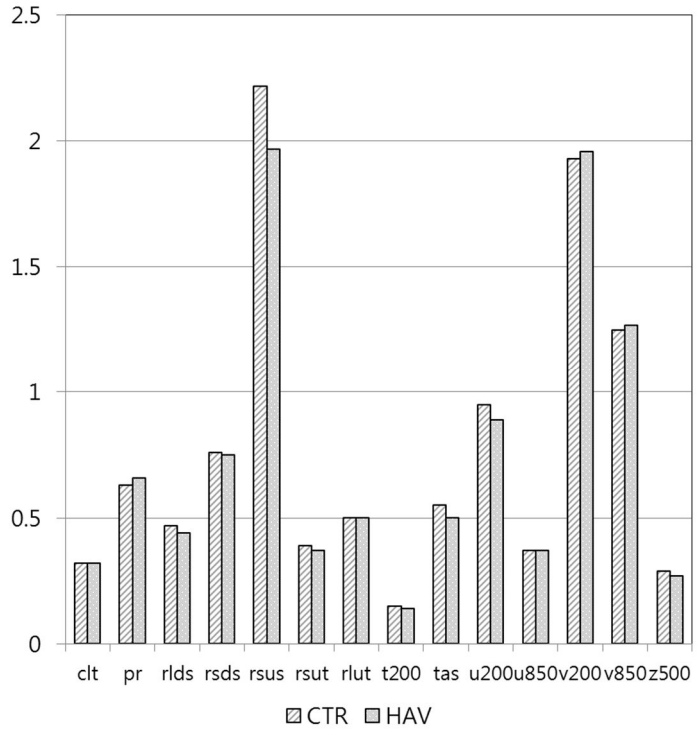

Figure 2.4. A comparison of the model performance index for control (CTR) and harvesting (HAV) conditions over East Asia (100–145°E, 20–50°N) for the period 1984–2005. Climate variables are total cloudiness (clt); precipitation (pr); up/down shortwave/longwave surface radiation (rlds, rsds, rsus, rsut, and rlut), temperatures at 200 hPa (t200), temperatures at 1.5 m (tas), wind at 200 and 850 hPa (u200, v200, u850 and v850), and geopotential at 500 hPa (z500).

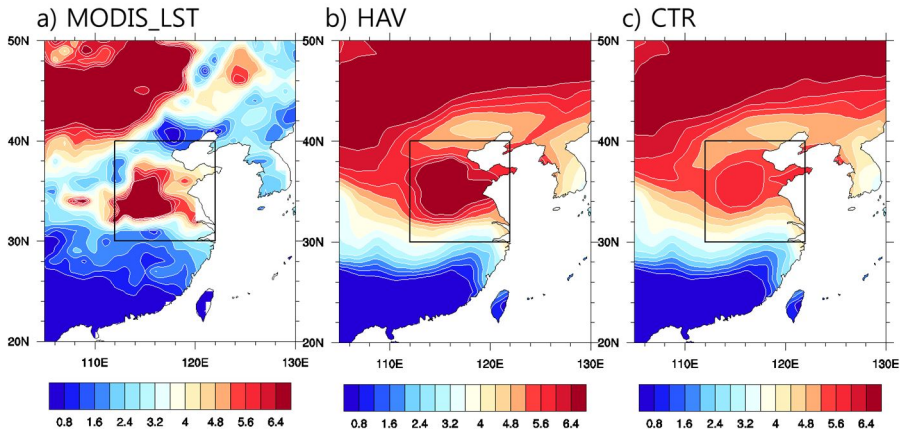

Figure 2.5. Changes in monthly surface temperatures (°C) (June versus May) from (a) MODIS LST for the period 2000-2006, (b) HAV, and (c) CTR for the period 1984–2005. The rectangular box in each panel denotes the analysis domain used in this study.

2.4.2 Effects on Land Surface Processes in Present

Ensemble average of monthly mean surface temperatures of the CTR and HAV were compared with MODIS land surface temperature

(LST) data for the period 2000–2006. The MODIS LST dataset contains global monthly mean daytime LST values averaged within 1° × 1° gridded cells. The MODIS LST values ranged up to 6°C higher in June than in May (Figure 2.5a). Despite of the prevalent cloud contamination caused by East-Asian summer monsoon, this warmer surface is in accordance with the observed station data in Figure 2.3a), and the correlations between the MODIS LST and the station observations were found to be statistically significant within 95% confidence level [Ho et al., 2012]. The simulated surface temperatures from the HAV showed more similar magnitude of change to those of the observed values (Figure 2.5a), than the results from the CTR (Figures 2.5c). After harvest, surface warming related to land surface conversion in Figure 2.5b was consistent with the results based upon observations [Ge , 2010; Ho et al., 2012] and model simulations [Cooley et al., 2005;Nair et al., 2007], which reported that the warmer

and drier surface climate response during the harvesting period was related to evapotranspiration from vegetation.

It must be noted that the results presented in the figures from this section were obtained by calculating the difference between the harvest and control runs. Statistical tests were performed to determine the significance of differences in means between control and harvest experiments and the tests include a student's t-test. The shaded regions in figures that follow display the confidence levels, which indicate that the differences exceeded the 95% confidence level.

After harvesting winter wheat, changes in the land surface caused by bare soil can affect the partitioning of energy into latent and sensible heat fluxes. Accordingly, the leaf area decreased and evapotranspiration from the canopy was reduced. Reduced evapotranspiration induced a decrease in latent heat flux from the surface to the atmosphere (Figures 2.6a and 2.6b), which contributed

to surface warming and air temperature. These results are consistent with many previous studies that state a decrease of latent heat flux can contribute to surface warming [Narisma and Pitman, 2003; Cooley et al., 2005; Ray et al., 2006; Ge, 2010; Jeonget al., 2011; Lee et al., 2011; Ho et al., 2012]. A similar result can be deduced from data in Strengers et al. [2010], which showed that increases in evapotranspiration can induce a cooler surface. A study that used a regional climate model [Xuejie et al., 2003] found that the increase in daily maximum temperatures caused by land use change was mainly due to the change from forest to crop cover over the northern region of China. Most studies agree that the presence of tropical forests can increase precipitation and cool the local climate compared to areas with lower amounts of vegetation, and these effects are mainly due to enhanced evaporative cooling [Hoffmann and Jackson, 2000; Roy et al., 2007; Bonan, 2001]. Active vegetation is known to enhance

transpiration, which results in cooler surfaces [Jeong et al., 2011]. In this study, the cooling effect of vegetation was likely inhibited because of a decrease in the latent heat flux caused by the removal of vegetation.

Table 2.4. Diurnal variation induced from harvest.

	Tmax(K)	Tmin(K)	Diurnal Temperature Range (K)
HAV	28.65	19.56	9.09
CTR	28.13	19.24	8.89
HAV-CTR	0.52	0.32	0.2

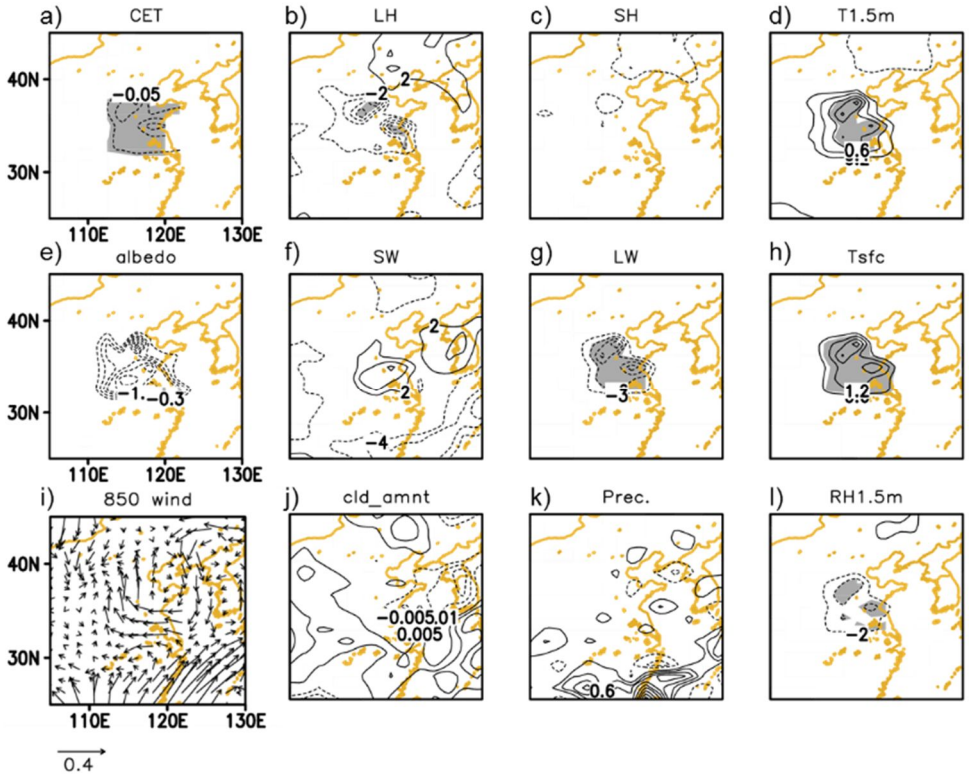

Figure 2.6. Differences between HAV and CTR results for June during the period 1984–2005. The variables are (a) evapotranspiration from the canopy (mm/day); (b) latent heat flux (W/m^2); (c) sensible heat flux (W/m^2); (d) 1.5 m air temperatures (°C); (e) land albedo (%); (f) short-wave radiation (W/m^2); (g) long-wave radiation (W/m^2); (h) surface temperature (°C); (i) horizontal wind at 850 hPa (m/s); (j) cloud amount (%); (k) precipitation (mm/day); and (l) relative humidity (%). The shaded area indicates the 95% confidence level.

The decrease in latent heat flux can lead to the repartitioning of available energy. In this study, the decreases of latent heat flux in June after harvesting were found to be much larger than the changes in sensible heat flux (Figure 2.6c). In addition to the changes in vegetation type and land surface properties, the albedo was also affected, which relates to the absorption of energy at Earth's surface. Difference of the albedos between the experiments, HAV and CTR, is resulted from the difference of fractional coverages of soil and crop. The area averaged snow free albedos used for soil and crop in the simulations are about 0.15 and 0.2, respectively: which results in about 0.009 (1%) change for the absorbed solar radiation at the surface (Figure 2.6f). Albeit the change is relatively small compared to the changes in evapotranspiration, it is not negligible when used in the heat balance. An increase in shortwave radiation (Figure 2.6f) also contributed to the rise in temperatures. Similar result were shown in

Strengers et al. [2010] and Narisma and Pitman [2003], where it is mentioned that in the subtropics, changes in evapotranspiration and the corresponding changes in latent heat flux and cloud formation can be more important than the albedo effect. Additionally, as given by Narisma and Pitman [2003] about impacts of land surface change on local air temperature, contribution of the latent heat flux couldbe larger those of albedo.

The decrease in latent heat flux induced an increase of the surface temperature and the emittance of long wave radiation (Figure 2.6g) to the atmosphere. It must be noted that upward long wave radiations have negative signs in the Figure 2.6, 2.9 and 2.10. However, the large decreases in latent heat flux out-weighed the increase in outgoing long wave radiation. As a result, the surface temperature and 1.5 m air temperature is warmed by 1.0°C and 0.4°C, respectively (Figures 2.6h and 2.6d). These changes in surface air

temperature are consistent with the changes in evapotranspiration and latent heat flux. It could, therefore, be inferred that harvesting in double-cropping areas creates a warmer and drier land surface. Although shortened roughness lengths caused by deforestation can be substantial [Hoffmann and Jackson, 2000; Sen et al., 2004; Kang and Hong, 2008; Takata et al., 2009], the change of roughness length caused by harvesting in this study appeared to be insignificant and very small. In MOSES2 scheme, roughness lengths for soil and crop are a constant, 3×10^{-4} m, and canopy height divided by a factor, respectively. As the area averaged canopy height for C_3 over the NCP was 0.76 m, the difference between the two experiments results in about 0.015 m, which might be negligible.

The results showed insignificant changes of cloud cover and precipitation over the NCP (Figures 2.6j and 2.6k). Simulated rainfall showed slight increases in precipitation to the south of 30°N (Figure

2.6k), which were associated with the anomalous convergence of low level horizontal winds (Figure 2.6i). Relative humidity was decreased by 2.3% due to harvesting, which was accompanied by the decreases in canopy evapotranspiration (Figure 2.6l), and the magnitude was a little smaller but had the same sign with the observations (Table 2.2, Figure 2.3b). It is consistent previous studies that assessed the drier surface after harvesting [Cooley et al., 2005; Ho et al., 2012].

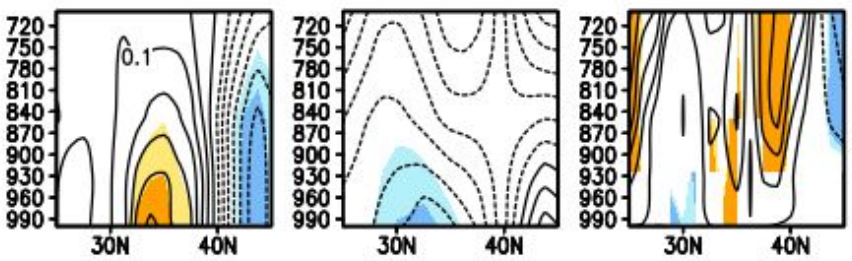

Figure 2.7. Height-latitude cross section of the difference between HAV and CTR results of the (a) temperature, (b) geopotential height and (c) vertical motion, averaged over the longitude 112 °E- 122 °E.

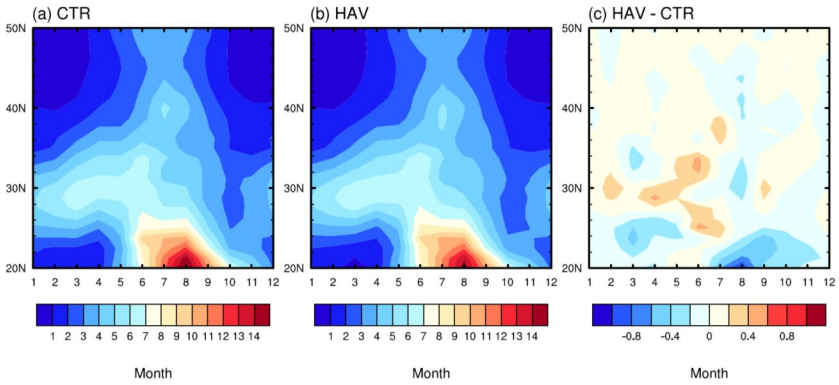

Figure 2.8. Time (Month)-latitude cross sections of monthly precipitation (mmday-1) over 110 E-120 E for (a) CTR and (b) HAV and (c) HAV-CTR.

The height-latitude cross section averaged over the longitude 112 °E- 122 °E showed that surface warming and upward motion over NCP region induced from harvest (Figure 2.7).

The temporal evolution of the East Asian summer monsoon (EASM) was examined through time-latitude distribution of precipitation. The time series of the precipitation averaged over 112 °E – 122 °E is shown in Figure 2.8. It was shown that HAV run simulated more precipitation over mid-latitude region before July. It

tends to simulate more rainfall in HAV run both in present and possible future.

In a view of surface energy balance, the relationship between residual energy from the surface energy budget equation and the skin temperature over NCP was examined (Figure 2.11). The surface (skin) temperature and the residual radiation showed the linear relationship.

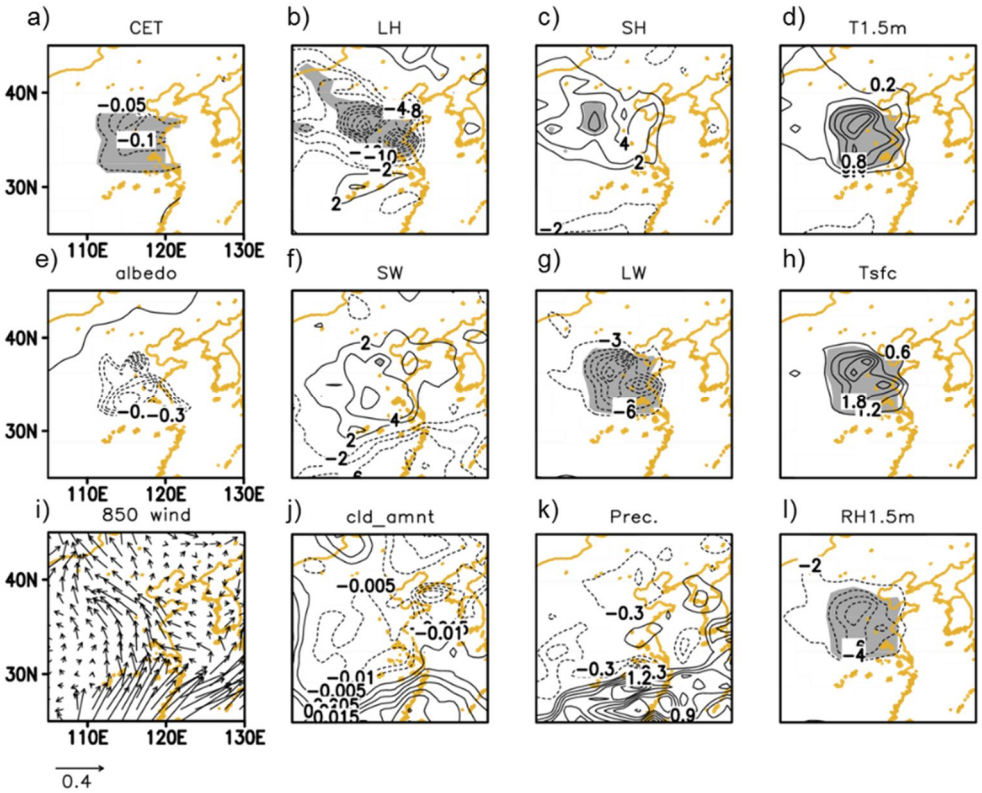

Figure 2.9. The same variables as Figure 2.6, but for HAV26 and CTR26.

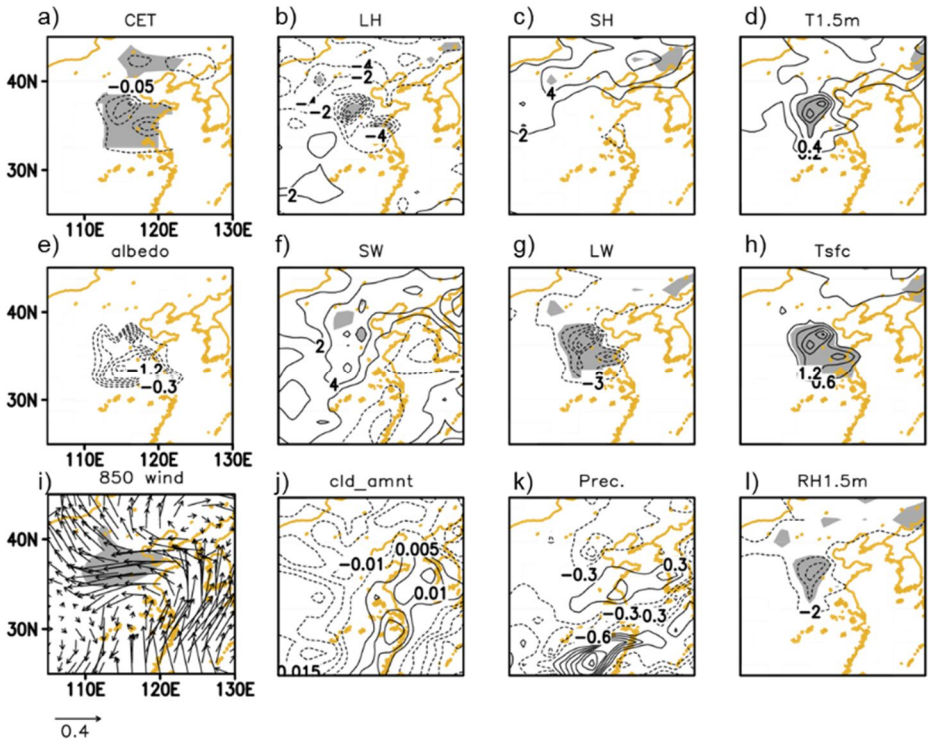

Figure 2.10. The same variables as Figure 2.6, but for HAV85 and CTR85.

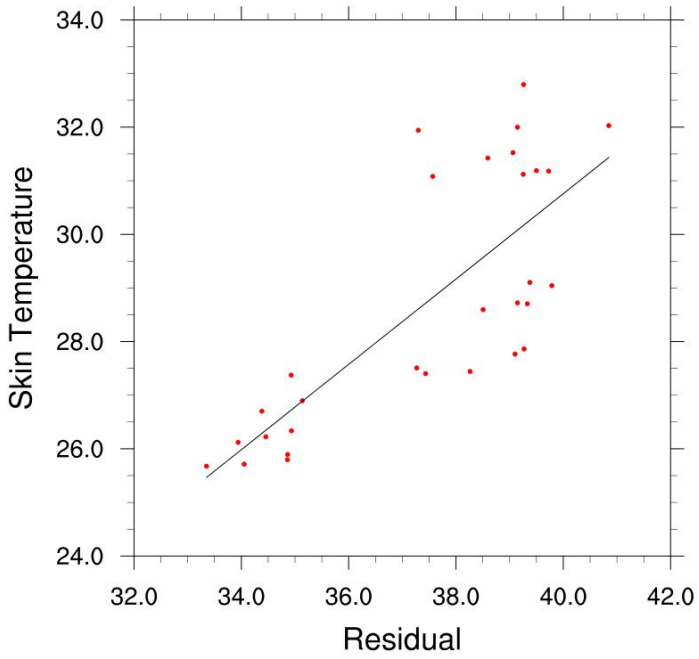

Figure 2.11. Skin temperature – surface residual energy averaged over North China Plain.

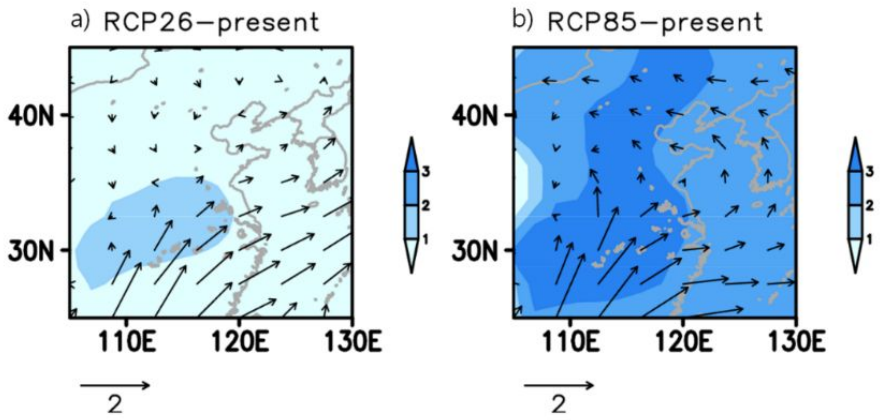

Figure 2.12. Changes in horizontal wind (vector, m/s) and specific humidity (shading, g/kg) at 850 hPa level for the period of 2071-2090 relative to 1984-2005 for a) the RCP 2.6 and b) the RCP 8.5 scenarios.

2.4.3 Effects on Land Surface Processes in Possible Future

To estimate possible future regional climate responses to surface changes during the harvest period in double-cropping systems, climate projections under the RCP 2.6 and 8.5 scenarios were evaluated. The combined effect of CO_2-induced warming and land surface change is important on a regional scale [Feddema et al., 2005; Pitman and Narisma, 2005; Pitman et al., 2011; Lawrence et al., 2012]. The RCP 2.6 scenario maintains that Earth will show some level of resilience. The RCP8.5 scenario combines assumptions of high population growth and relatively slow income growth with modest rates of technological change and energy intensity improvements, which are predicted to lead in the long-term to high energy demands

and GHG emissions in the absence of climate change policies [Moss et al., 2010].

Under the future warming conditions of both the RCP 2.6 and RCP 8.5 scenarios, the surface climate response after harvest in the NCP is shown in Figures 2.9 and 2.10. It can be seen the changes affected by the GHGs and SSTs through comparing CTR and CTR26 and CTR85. According to the results from CTR26 and CTR85, 1.5 m air temperatures over the NCP were simulated to increase by 1.6°C and 5.1°C in 2071 to 2090 compared to 1984 to 2005. The relative humidity was simulated to decrease by 1.3% and 4.8% in 2071 to 2090 compared to 1984 to 2005 under the RCP 2.6 and 8.5 scenarios, respectively. Compared to the present-day run (Figure 2.6d), under RCP 2.6 scenario, the 1.5 m air temperature change between HAV26 and CTR26 over the NCP after harvest was simulated to increase by 0.7°C (Figure 2.9d). Under RCP 8.5 scenario, the 1.5 m air

temperature change averaged over the NCP between HAV85 and CTR85 was 0.4°C (Figure 2.10d). The surface temperature changes caused by land surface conversion showed that additional warming of 1.4°C and 1.0°C is possible under the RCP 2.6 and 8.5scenarios, respectively (Figures 2.9h and 2.10h). In other words, these results show that land surface conversion has the potential to enhance the projected warming from the GHGs effect by up to 1.4 °C. The systematic temperature signal associated with each experiment (Figure 2.9 and Figure 2.10) is noteworthy and gives us confidence that the results are robust. However, the warming effect of the land surface type conversion declines as warming intensifies such that by RCP 8.5, even the harvest under RCP 8.5 only warms by 1.0 °C. Relative humidity decreased by 4.6% and 2.2% in RCP 2.6 and 8.5, respectively (Figures 2.9l and 2.10l). Surface temperature and relative

humidity changes between HAV26 and CTR26 due to harvesting were larger than those between HAV85 and CTR85.

The warming effect of harvest in the NCP was mainly due to a decrease in the latent heat flux. The processes that induced a warm and dry surface climate in June under the RCP 2.6 and RCP 8.5 scenarios were consistent with the results from present-day simulations (Figure 2.6). The reduction of evapotranspiration and latent heat flux, which were associated with increases in sensible heat flux, appear significant in Figures 2.9a–2.9c. Albedo and increased incident radiation in Figures 2.9e, 2.9f, 2.10e, and 2.10f showed more significant changes with those in Figure 2.6. Adding the effects of land cover change to the Special Report on Emissions Scenarios (SRES) was also evaluated in Feddma et al. [2005], who observed a similar relationship between latent heat flux and temperature. Even though the results from their study show that the enhanced impact is

regional and corresponds to the tropical region, the results in this study suggest that the impact of crop practices on climate are comparable to those from land cover change demonstrated in other studies [Bonan 2001; Feddema et al., 2005; Pitman and Narisma, 2005; Pitman et al., 2011; Lawrence et al., 2012].

Under the different GHGs induced warming conditions in the RCP 2.6 and 8.5 scenarios, a comparison between control and harvest runs showed a similar response of additional warming by the surface climate to the land type conversion. In RCP 2.6, the additional rise in surface temperature between HAV26 and CTR26 (1.4 °C) was comparable in magnitude to the GHGs induced warming between CTR26 and CTR (1.6 °C). However, for RCP 8.5, the additional rise in surface temperature between HAV85 and CTR85 (1.0 °C) was much smaller than the GHGs induced warming between CTR85 and CTR (5.1 °C). The magnitude of difference between the harvest run and

the control run was also smaller in RCP 8.5 than in RCP 2.6. This is consistent with results from Pitman et al. [2011], which showed that the impact of LULCC depends on background regional climate conditions that are strongly affected by the level of CO_2. The difference is likely related to changes in the amount of cloud cover and precipitation. In Figures 2.10j and 2.10k, the RCP 8.5 scenario was simulated slightly larger cloud amounts and precipitation with the inflow of Figure 2.10i than that of RCP 2.6 in Figures 2.9j and 2.9k. Furthermore, the wetter conditions under RCP 8.5, as opposed to those in RCP 2.6, seem to suppress surface warming. The GHGs and SSTs induced changes of low level wind and moisture at the ends of 21st century under RCP scenarios were shown in Figure 2.12. Both scenarios showed increased specific humidity over the NCP, but the moisture advection toward the NCP was stronger under RCP 8.5 than under RCP 2.6. These results reflect the fact that responses to land

surface change in an extra-tropical climate are the results of a mixture of local land surface change effects and changes in the large scale circulation [Feddma et al., 2005; Pitman et al., 2011].

Chapter 3. The impacts of land cover generated by dynamic vegetation model and dust direct radiative effects on East Asian climate

3.1 Backgrounds

Bordered by the Tibetan Plateau to the west, the Eurasian land mass to the northwest, and the vast Pacific Ocean to the south and east, East Asia has experienced one of the most pronounced monsoon climates of the globe for centuries (Lau and Li, 1984). Land surface properties are important because of their known impact on the East Asian monsoon circulation (Kang and Hong, 2008; Lee et al., 2011) and on the Indian monsoon (Douglas et al., 2006; Lee et al., 2009; Bayer et al., 2012; Martin and Levine, 2012). Lee et al. (2011) proposed

that a replacement of vegetation with bare soil would cause an associated decrease in latent heat during the summer, which could weaken East Asian monsoon circulation. This decrease in latent heat flux over land could weaken the East Asian monsoon via a positive feedback between the latent heat flux contrast and rainfall. Yamashima et al. (2011) showed a similar study over the Indian subcontinent and Southeastern China. Land surface property changes from forest to cultivated land have resulted in a decrease in the monsoon rainfall and provoked an associated weakening of the Asian summer monsoon circulation. Moreover, there are a few studies investigating the influence of land cover change that have demonstrated significant impact on East Asian Monsoon (Kang et al., 2005), but they usually used satellite-based (Suh and Lee, 2004; Kang and Hong, 2008) and idealized land cover change (Lee et al., 2011).

Although Earth System models with dynamic vegetation schemes allow representation of the carbon cycle feedbacks on climate, the land cover distribution could also be influenced by, and indeed influence, model systematic biases (Martin and Levine, 2012, hereafter ML12). Land surface property changes have effects on the atmosphere through physical processes (such as changes in surface roughness, albedo and evapotranspiration), and can induce additional indirect impacts when coupled with aerosol processes as well. For example, changes in surface emissions of mineral dust that are caused by changes in bare soil fraction will have a radiative effect in the atmosphere. Additional dust loading of the atmosphere resulting from land cover change in an Earth System model could, therefore, add to the model uncertainty via feedbacks with model systematic biases such as lack of rainfall over dust-producing regions. Dust affects both shortwave and longwave radiative fluxes, and the

effects of mineral dust on the radiation budget are important due to the widespread distribution and large optical depth of mineral dust (Sokolik and Toon, 1996). A study by Yoshioka et al. (2007) suggests that the direct radiative forcing of dust can explain up to 30% of the observed precipitation reduction in the Sahel in three decadal scale simulation. Dust is removed from the atmosphere by both dry and wet deposition processes, providing a source of iron to phytoplankton and thus potentially affecting the carbon cycle (Collins et al., 2011). Since Northeast Asia is one of the major dust emission source regions, land surface property changes over this source region need to be studied. Aerosol, as one of the fundamental atmospheric constituents, has an important impact on the climate system. Ramanathan et al. (2005) showed that global dimming causes a long-term (multi-decadal) weakening of the South Asian monsoon by reducing the meridional surface temperature gradient between the

Asian land mass and the Indian Ocean. Aerosol affects precipitation events through cloud physics processes in China (Qian et al., 2009), while dust can also contribute to Asian monsoon rainfall anomalies by heating the upper troposphere (Lau et al., 2006, Lau and Kim, 2006).

ML12 investigated land surface and dust impacts in terms of the feedback between model systematic biases. Their results reflect that over dust producing regions, land cover change simulated by a Dynamic Global Vegetation Model (DGVM) can affect both the present-day simulation and the future response as well. According to Hurrel et al. (2009) and McCarthy et al. (2012), since model systematic biases affect climate model sensitivity, we need to study processes related to systematic biases in order to understand future climate projections. Motivated by ML12, this study extends ML12 by applying their results for East Asia. The aims of this study are: first,

to investigate the physical influence of land cover conditions and associated aerosol loading on the rainfall and surface temperature over East Asia; and second, to provide insight into the contribution of uncertainty in modeling of land cover changes to the uncertainty in future climate projections of rainfall land surface temperature for the region.

3.2 Model Experimental Design and Data

In this study, they were used the ML12 datasets which were performed using the Hadley Centre Global Environmental Model version 2 (HadGEM2) model family that had been developed by the UK Met Office (The HadGEM2 Development Team, 2011). The horizontal grid interval was 1.25°x1.875° in the latitude-longitude

directions, and 38 vertical layers were used with the top of atmosphere over 39 km in height. The land surface scheme in the HadGEM2 family is a tiled version of the Met Office Surface Exchange Scheme (MOSES) version 2, which represents heterogeneous surface properties (Cox et al., 1999; Essery and Clark, 2003). A grid box represents a mixture of five vegetation or plant-functional types (PFTs), which include broadleaf trees, needleleaf trees, temperate C3 grass, tropical C4 grass, and shrubs, and four non-vegetated surface types, which include urban, inland water, bare soil, and ice. Surface fluxes and temperatures are calculated separately for each surface type and are aggregated according to each tile's fractional coverage before being passed to the atmospheric model (Lawrence and Slingo, 2004).

The experiment configuration is as follows. For the present-day (1980-2005) runs, the HadGEM2 atmosphere-only model was forced

with observed sea surface temperatures (SSTs) and sea ice. The experimental design and forcing datasets are as specified by the Fifth Coupled Model Intercomparison Project (CMIP5; Taylor et al., 2012) and are detailed in Taylor et al. (2012). The land cover and vegetation types were prescribed by the International Geophysical Biophysical Programme (IGBP; Loveland et al., 2000) with a prescribed seasonally-varying leaf area index (LAI) based on Moderate Resolution Imaging Spectroradiometer (MODIS) Terra Collection 5 monthly LAI datasets. Historical land use change information based on CMIP5, provided to CMIP5 by the Land Use Harmonization team (Hurtt et al., 2011), were applied by Baek et al. (2013) to the IGBP land cover data in order to prescribe time-varying land cover fields for HadGEM2-A. This is referred to as the "A" experiment.

For the future timeslice experiments, the atmosphere component is forced with CO2 and trace gases for the year 2100

based on the Representative Concentration Pathway (RCP) 8.5 scenario of the CMIP5. The SSTs were obtained by applying the difference between 30-year mean SSTs centred around 2100 (from the HadGEM2 Earth System (HadGEM2-ES) RCP8.5 scenario coupled model run) and 30-years mean SSTs centred around 1990 (from the HadGEM2-ES historical run), to the present-day monthly-varying observed SSTs from 1980–2005. The projected future land use changes for the period 2080-2110 based on CMIP5 RCP8.5 scenarios were applied in order to prescribe time-varying land cover fields for HadGEM2-A timeslice experiment. This is referred to as the "Ats" experiment.

In addition to the "A" and "Ats" experiments, alternative representations of global vegetation cover from a DGVM were used as the land cover component for further HadGEM2-A experiments under present-day and future climates. In these experiments, the

monthly mean land cover information from the HadGEM2-ES historical and RCP8.5 runs are used in HadGEM2-A in place of the standard land cover distribution as described above. The HadGEM2-ES configuration uses the Top-down Representation of Interactive Foliage and Flora Including Dynamics (TRIFFID) dynamic vegetation model (Cox, 2001) to simulate the land cover changes from the pre-industrial control period through the present-day and into the future following the CMIP5 RCP scenarios, and land use changes from Hurtt et al. (2011) are applied as disturbances (see Jones et al., 2011 for more details). Therefore, in these additional experiments, the variations in land cover with time during these periods in HadGEM2-ES are experienced by HadGEM2-A, but there is no interactive terrestrial carbon cycle and no feedbacks on the land cover. Variations in land cover from years 1980–2005 of HadGEM2-ES are used in the present-day experiment of this type, referred to as "AE", while the

variations in land cover from years 2080-2110 of HadGEM2-ES are applied to the future timeslice experiment denoted “AEts”.

According to ML12, the AE experiment shows a large increase in dust, which is generated as a result of the additional fraction of bare soil occurring in HadGEM2-ES as a result of the feedback between the interactive vegetation and the model’s systematic rainfall biases in dust-producing regions. To evaluate the radiative effects of the dust, an additional pair of experiments was carried out where the direct radiative effects of the dust were switched off. These experiments have the suffix “nod” meaning “no dust radiative effects”. Therefore, “Anod” means a HadGEM2-A simulation with the standard land cover distribution in the present-day, “AEnod” means a HadGEM2-A present-day simulation with HadGEM2-ES land cover without the direct radiative effects of the dust, and “AEnodts” means a HadGEM2-A future timeslice simulation with HadGEM2-ES land

cover without the direct radiative effects of dust. The total experiments are listed in Table 3.1.

To compare model results in the present-day runs with observations we used the Global Precipitation Climatology Project (GPCP) precipitation (Alder et al., 2003; Huffman et al., 2009), the CPC Merged Analysis of Precipitation (CMAP, Xie and Arkin, 1997) and the Climatic Research Unit (CRU) mean surface air temperature (Harris et al., 2013). In this study, summer represents the period from June to August.

Table 3.1. List of experiments.

Acronyms for the experiments	Descriptions of the experiments	Time
HG2AE_nodust	HadGEM2-A with ES vegetation with no dust radiation	Present 1980-2005
HG2A_nodust	HadGEM2-A with no dust radiation	
HG2AE	HadGEM2-A with ES vegetation	
HG2A	HadGEM2-A	
HG2AE_ts	HadGEM2-A with ES vegetation time slice run	Future 2080-2110
HG2AE_nodts	HadGEM2-A with ES vegetation time slice run with no dust radiation	
HG2A_ts	HadGEM2-A time slice run	

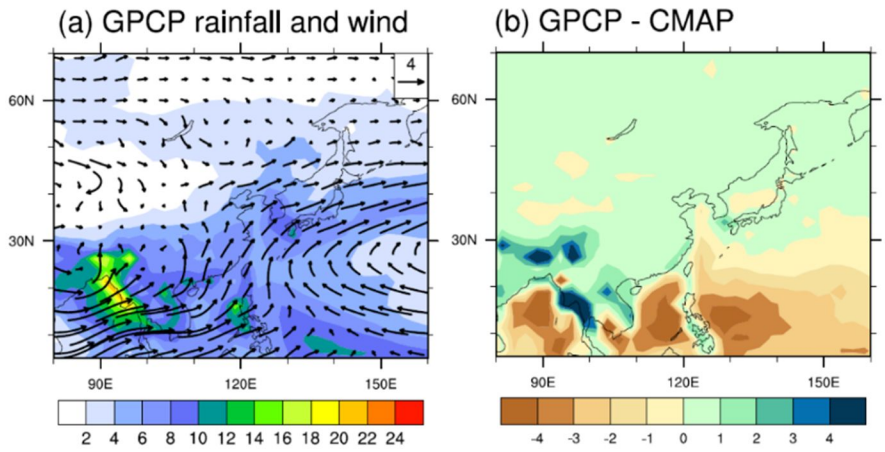

Figure 3.0. The 1982-2005 (a) climatology of the Global Precipitation Climatology Project (GPCP) precipitation (mm day^{-1}, shading) and 850hPa winds (m s^{-1}) and (b) precipitation difference between GPCP and the CPC Merged Analysis of Precipitation (CMAP) in JJA.

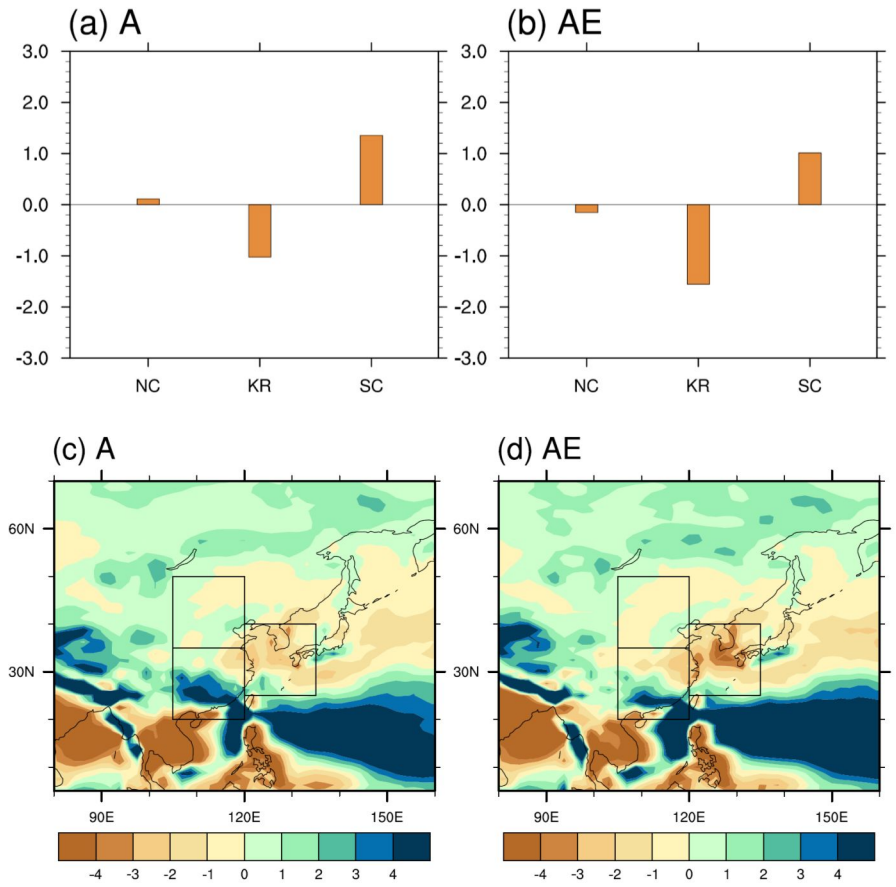

Figure 3.1. Area averaged precipitation bias (mm day^{-1}) compared to observation in JJA: (a and b) show regional mean biases over the regions shown in (c and d). NC region: 35-50° N, 105-120° E; KR: 25-40° N, 120-135° E; SC region: 20-35° N, 105-120° E.

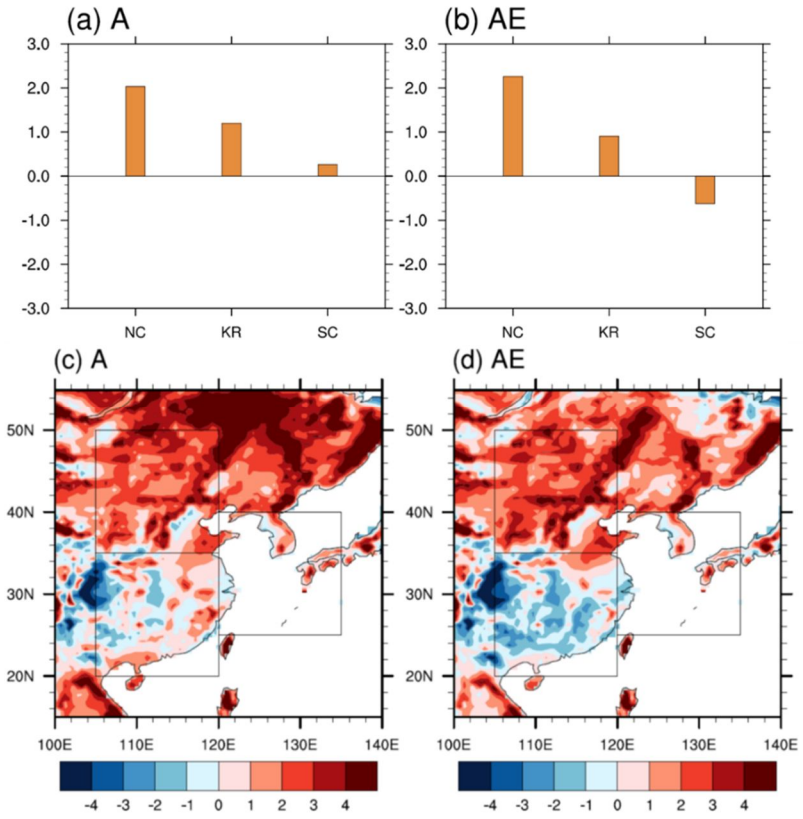

Figure 3.2. As Fig. 3.1 but for JJA surface air temperature biases (K) compared to the Climatic Research Unit (CRU) climatology.

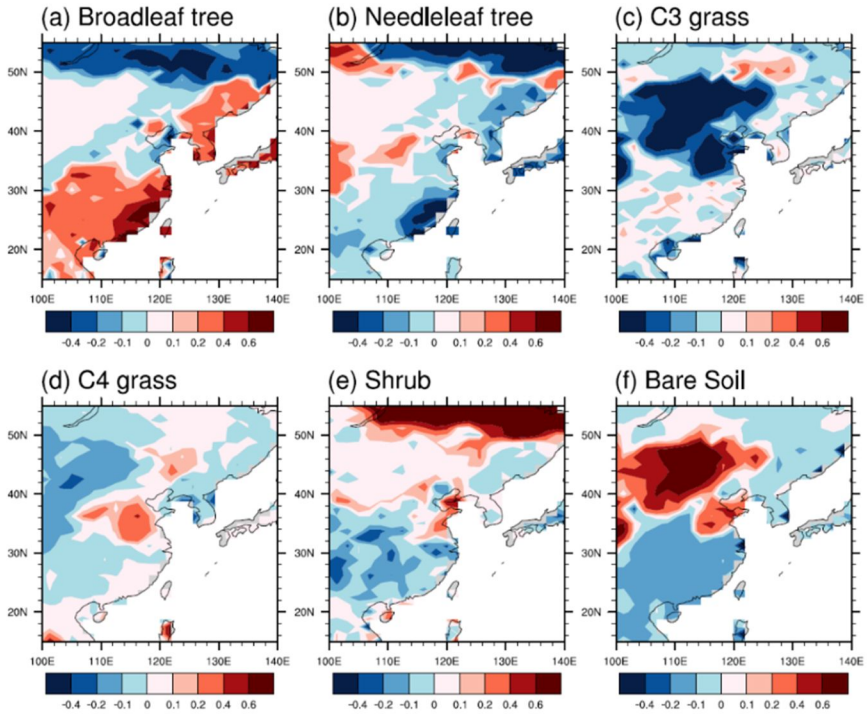

Figure 3.3. Differences in present-day (1980-2005) land cover type between HadGEM2-ES and HadGEM2-AO (and HadGEM2-A) over East Asia.

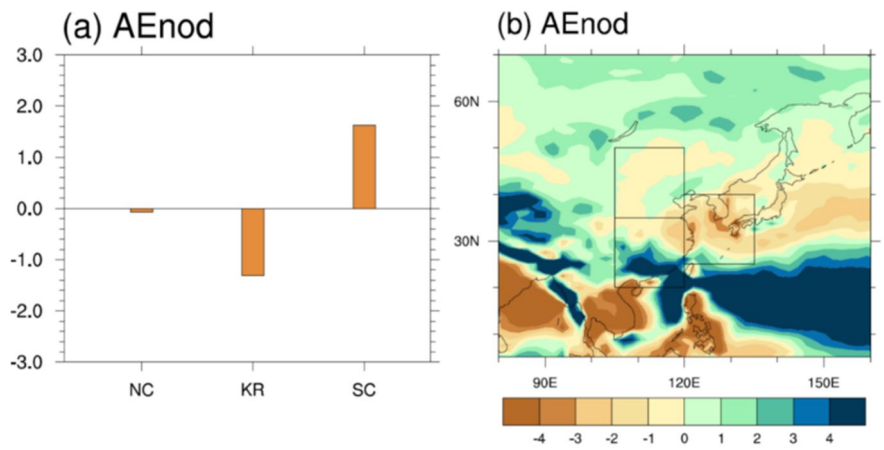

Figure 3.4. Summer (a) area averaged precipitation bias (mm day^{-1}) compared to observation and (b) horizontal distribution of precipitation bias, in HadGEM2-AE simulation without the direct radiative effect of dust.

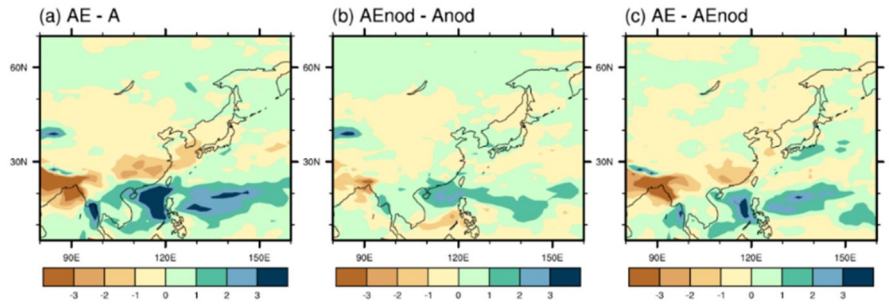

Figure 3.5. Precipitation differences (mm day^{-1}) in summer for (a) AE minus A (b) AEnod minus Anod, and (c) AE minus AEnod.

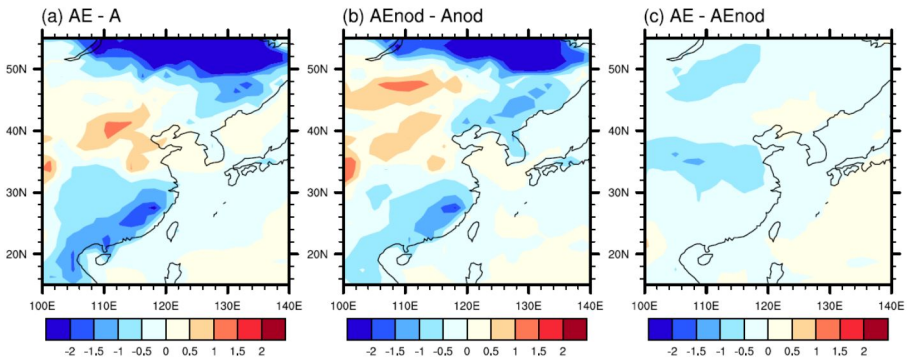

Figure 3.6. Surface air temperature differences (K) in JJA for (a) AE minus A, (b) AEnod minus Anod, (c) AE minus AEnod.

3.3 Modeling Results

3.3.1 Present Day

3.3.1.1 Impact of ES land cover on Average Temperature and Precipitation

First we examine summer precipitation over East Asia. Figure 3.0a shows the typical summertime precipitation distribution of the East Asian summer monsoon. The summer monsoon rainy season evolves with the rainband development covering South China, Korea, Japan and the adjacent seas. Formation of frontal systems is associated with the North Pacific Subtropical High and

southwesterlies over the South China Sea. The rainband region, contrasting to the equatorial region, corresponds to have small observation uncertainty (Fig. 3.0b). In Fig. 3.1, we analyzed the North China (NC) region (35-50^{o} N, 105-120^{o} E), Korea (KR) 25-40^{o} N, 120-135^{o} E, and South China (SC) region (20-35^{o} N, 105-120^{o} E) which represent a large contrast in land cover distribution over East Asia. Simulated precipitation compared with observation (GPCP precipitation) shows a systematic bias in Fig. 3.1. Precipitation is underestimated over KR area and overestimated over SC. These spatial features remain in AE, although the underestimated rainfall over KR become larger in AE than A. Figure 3.2 represents summer surface air temperature bias in the model results compared with the CRU observation data. There is a warm bias greater than 1K in NC and KR, but only a small bias in SC (Fig. 3.2a). The warm bias over KR is slightly smaller in AE compared to A (Fig. 3.2c, d). In order to

shed light on the bias changes on the regional scale, the land cover difference between AE and A is examined (Fig. 3.3). Among the five vegetation and bare soil surface types over East Asia, the largest changes are in broadleaf, C_3 grass and bare soil types. Over North China, the increase in bare soil fraction is large. This unrealistic high bare soil fraction has an impact on high dust emission over this region because dust is only emitted from the bare soil fraction of a grid box in this model. On the other hand, the South China region is covered by larger broadleaf fraction (Fig. 3.3) in the AE compared with A, replacing bare soil, shrub and needle-leaf tree. To the north of 50^{o}N, the increase in shrub fraction is distinct (also seen in Fig. 3.4 of ML12).

ML12 showed that bare soil area expansion from the changes in the vegetation distribution between AE and A generates additional dust, resulting in a substantial direct radiative impact on the Indian

monsoon rainfall. They suggest separate analysis for the dust radiative feedback from the response to land cover change. Accordingly, we examine experiments Anod and AEnod (see Table 1).

In Fig. 3.1, a marked precipitation underestimation over KR is shown compared with observation, particularly when the ES land cover is used. The dry bias amplitudes in summer become larger in AE compared with A (Fig. 3.1). To estimate the radiative effect of dust on rainfall when the HadGEM2-ES land cover distribution was used, AE was compared with AEnod. The dry bias amplitude of AE decreases in AEnod (Fig. 3.4) but is still slightly larger than in A. Thus the radiative effect of dust reinforces the dry bias in the KR region (compare Fig. 3.1(b and d) with Fig. 3.4). This is consistent with the results of ML12 for the South Asian region.

To examine the dust radiative effect and land cover change effect in detail, the dry bias in summer over KR in Fig. 3.1 and 3.4 is

considered using Fig. 3.5. The pattern of changes between AE-A in Fig. 3.5a is similar to the "AE – AEnod" changes (Fig. 3.5c) rather than those of "AEnod – Anod" (Fig. 3.5b). This suggests that the radiative effects of changes in dust that are associated with the land cover changes are likely to be more important for simulating precipitation over East Asia than the changes in surface processes associated with the same land cover changes.

In Fig. 3.6 we make a similar comparison for surface air temperature changes. We find that the dust radiative effect on surface air temperature is associated with a small widespread cooling (Fig. 3.6c), whereas the surface process effects of the land cover change are associated with a more substantial warming/cooling pattern across the region, as shown in the AEnod-Anod (Fig. 3.6b) and AE-A (Fig. 3.6a) differences. Over northeastern Eurasia, the increase of shrub fraction replacing broadleaf and needleleaf trees shows a distinct

cooling of surface air temperature induced from an increase of surface albedo.

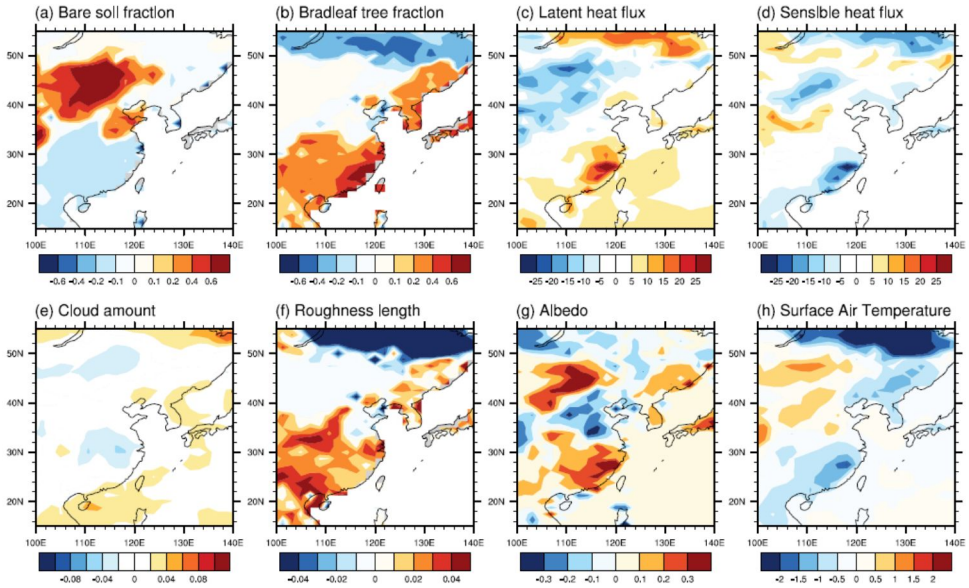

Figure 3.7. AEnod minus Anod in JJA showing the applied fractional land cover changes and their impact in (a) bare soil fraction, (b) broadleaf tree fraction, (c) latent heat flux (W m^{-2}), (d) sensible heat flux (W m^{-2}), (e) cloud amount (fraction), (f) roughness length (m), (g) albedo (%) and (h) surface air temperature (K).

3.3.1.2 Impact of Changes in Land Cover with No Dust Radiative Feedback

To understand more clearly the impacts of the changes in the vegetation distribution in Fig. 3.6a and 6b, we examined the climate response without the direct radiative effect of dust. The aforementioned increase in warm bias over NC "AEnod–Anod" (Fig. 3. 6b) is considered. Over NC, as the bare soil fraction is larger in AE than A (Fig. 3.3f; Fig. 3.7ab), the roughness length reduces while soil evaporation and canopy evaporation decrease. Reduced roughness length induces a decrease of sensible and latent heat fluxes from surface to the atmosphere (Fig. 3.7c, d, f). The decrease in latent heat flux is associated with reduced cloud amount (Fig. 3.7e), as well as being favorable for surface warming. As a result, surface air temperature rise (Fig. 3.7h). The reduced latent heat flux is

particularly evident in the canopy evaporation in the NC region (Fig. 3.8d), although there is also reduced soil evaporation during the summer (Fig. 3.8a).

Similarly, surface cooling over SC and KR is considered in summer. Broadleaf tree fraction expansion (Fig. 3.7b) increases the roughness length (Fig. 3.7f) and latent heat flux (Fig. 3.7c), driving surface cooling. Whereas the NC region where bare soil fraction is increased showed a decrease of evaporation from A to AE, in the KR and SC regions where broadleaf tree fraction is increased there is increased soil and canopy evaporation from A to AE (Fig. 3.8). These results are consistent with the suggestion by Lee et al (2011) that a vegetation replacement with bare soil would cause an associated decrease in latent heat during the summer. In summary, for the present climate, the land cover effect (bare soil fraction changes in Fig.

3.7a) is related with surface air temperature changes in summer (Fig. 3.7h). As soil fraction expands (shrinks) the temperature rises (drops).

As regards precipitation, Fig. 3.5 shows only very small changes in precipitation over land in AEnod-Anod (Fig. 3.5b). Thus, the model's direct sensitivity of precipitation to changes in land surface conditions seems to be low compared with the sensitivity to the dust changes that result from them.

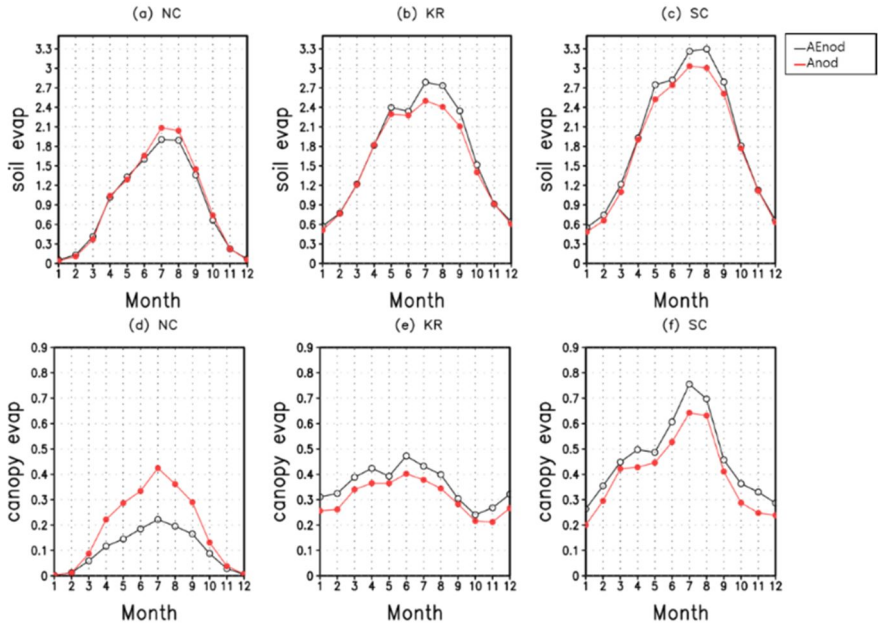

Figure 3.8. Monthly variation of soil and canopy evaporation (mm day^{-1}) in AEnod and Anod for the present-day simulation (1982-2005) over North China (NC), Korea (KR), South China (SC) region

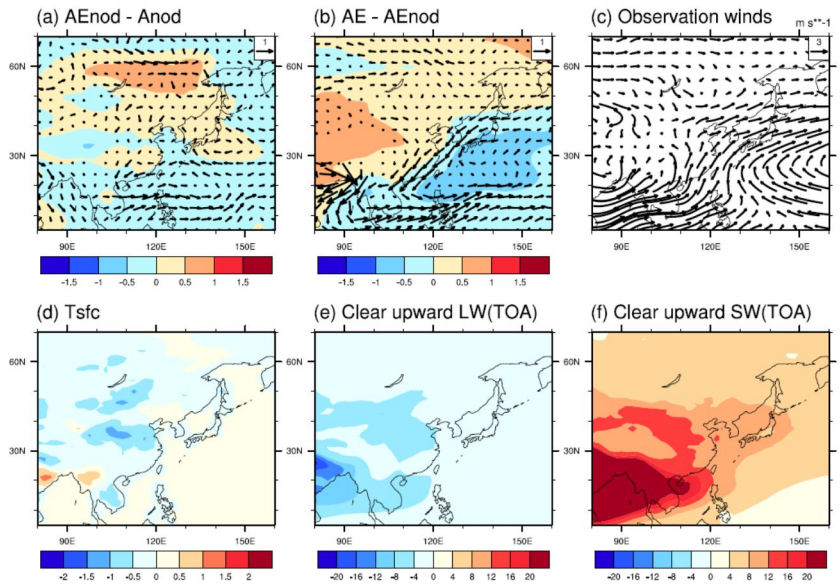

Figure 3.9. Changes in mean sea level pressure (hPa) and 850 hPa winds (m s^{-1}) in JJA for (a) AEnod minus Anod, and (b) AE minus AEnod. (c) Climatology of 850 hPa winds for the period 1982-2005 using ERA Interim; (d to f) show differences between AE and AEnod in JJA: (d) surface temperature (K), (e) clear sky upward longwave radiation (W m^{-2}) and (f) clear sky upward shortwave radiation (W m^{-2}) at top of atmosphere, showing the impacts of the radiative effects from additional dust loading induced by the ES land cover.

3.3.1.3 Impact of Dust Radiative Feedback

We now consider the direct radiative effect of dust resulting from the changes in the vegetation distribution (AEnod-Anod and AE-AEnod of Fig. 3.9). Concerning the regional climate response, the dust direct radiative effects (Fig. 3.9b) are represented by anomalous northeasterly coastal flow counteracting the summertime climatological monsoonal circulation associated with the western North Pacific high, known to be important in the East Asian summer monsoon rainfall (Lee et al. (2006) and Fig. 3.9c). The sea level pressure and wind anomalies in "AE - AEnod" are stronger than those of "AEnod - Anod" (Fig. 3.9a, b), illustrating that the radiative effects of the dust have a larger impact than the surface vegetation changes themselves.

The direct radiative effect of dust induces anomalous cyclonic flow over the western North Pacific (KR region in Fig. 3.9b) that

would decrease rainfall over East Asian continent. This is because dust reflects a considerable amount of shortwave radiation, as shown by the increase of upward shortwave radiation at the top of atmosphere (TOA; Fig. 3.9f), with a resulting cooling the land surface (Fig. 3.9d). The land surface cooling appears on the continental scale. This is somewhat different from the results in Miller and Tegen (1998) in which they mentioned that the reflected solar flux is offset by the absorption of upwelling longwave radiation, so that the net radiation entering the TOA is only weakly perturbed by dust in comparison to the surface reduction. Although the upward longwave flux is reduced through the dust radiative effects (Fig. 3.9e), the reduction is smaller than the increase in reflected shortwave at the TOA. Differential heating between land and ocean is one of the fundamental driving mechanisms of the monsoon (Webster et al., 1998). The land-sea thermal contrast becomes weaker due to the

direct radiative effect of dust and the pressure contrast weakens. Strong anomalous northeasterly flow along the coast (Fig. 3.9b), weakening the summer monsoon inflow, induces the dry bias over SC and KR (Fig. 3.5c). These results seems in line with the argument that dust-induced surface cooling is the dominant mechanisms leading to a reduction of precipitation (Konaré et al., 2008; Yoshioka et al., 2007; Paeth and Feichter, 2005).

Table 3.2. Impacts of climate change of global warming, land cover change and dust loading obtained by the difference between the experiments in this study.

Impact	Descriptions
Climate change (Global warming)	Ats – A
Climate change + LCC + Dust	AEts – AE
Climate change + LCC	AEnodts – AEnod
Dust	(AEts –AE) – (AEnodts – AEnod)
LCC (ES land cover)	(AEnodts – AEnod) – (Ats – A)

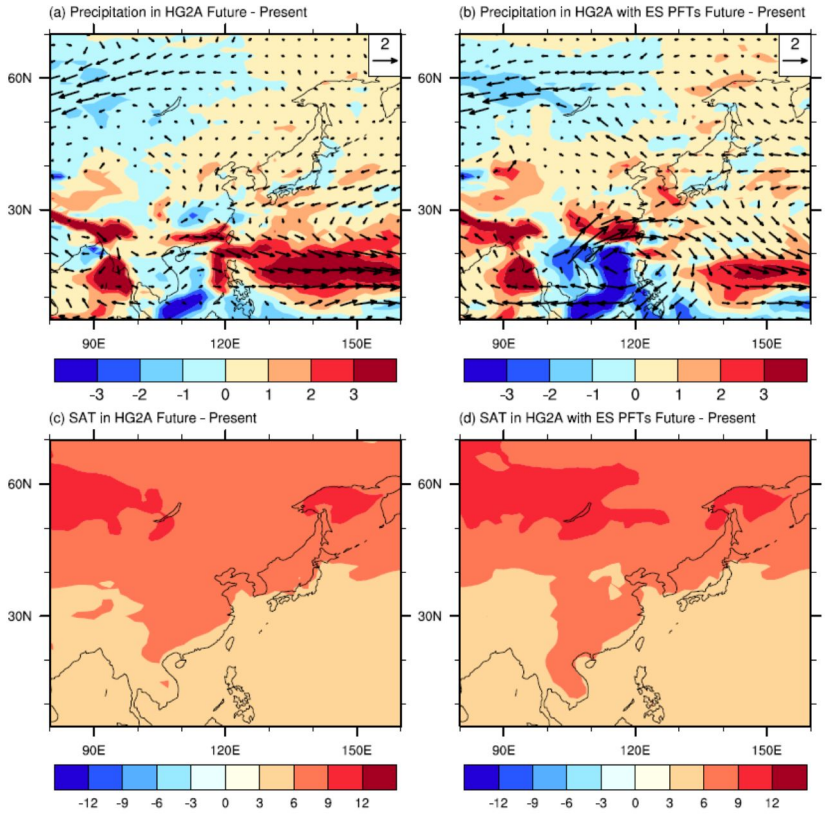

Figure 3.10. Changes in JJA mean precipitation (shading, mm day^{-1}) between future timeslice and present-day HadGEM2-A experiments, without (a, c) and with (b, d) land cover from HadGEM2-ES. (a), (c) is (Ats-A) and (b), (d) is (AEts-AE).

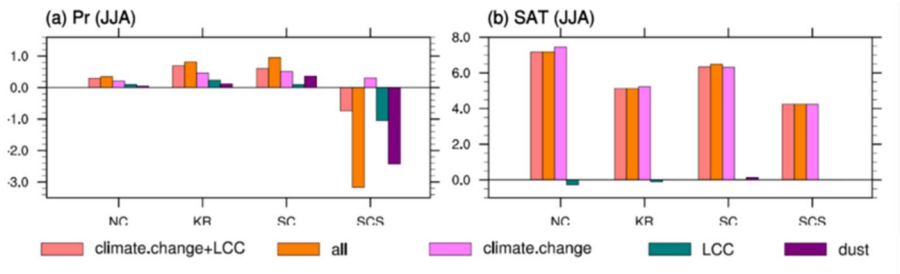

Figure 3.11. Future changes of precipitation (mm day^{-1}) (a) and surface air temperature (K) (b) over the box regions of North China (NC), Korea (KR), South China (SC) and South China Sea (SCS) in summer. Note that "all" means sum of climate change, land cover change and direct radiative effect of dust; "LCC" and "Dust" are 'double-differences' illustrating the influence of those processes on the future-present changes.

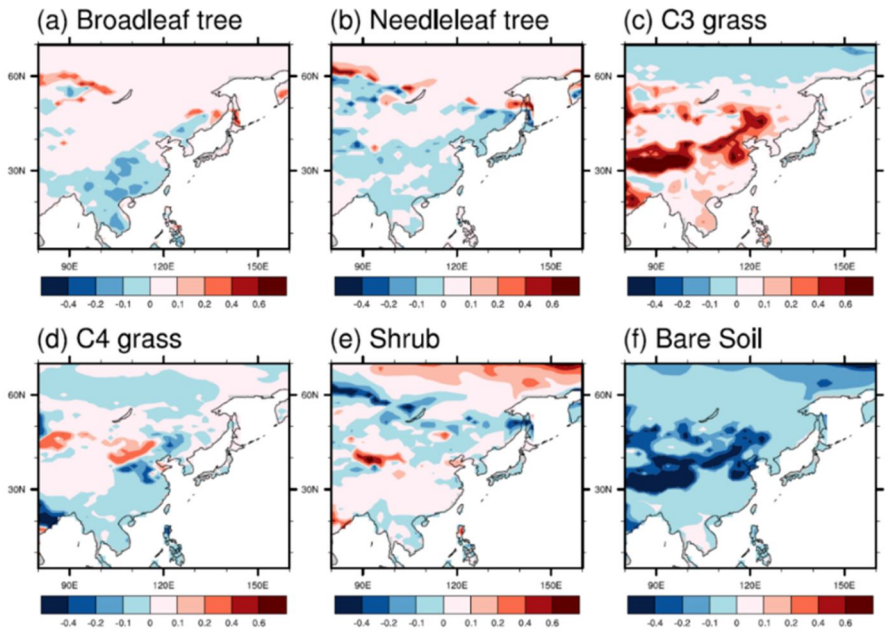

Figure 3.12. Changes in land cover between c.2100 and present-day as simulated by HadGEM2-ES in the Fifth Coupled Model Intercomparison Project (CMIP5) the Representative Concentration Pathway (RCP) 8.5 scenario and applied in AE present and AEts future time-slice experiments.

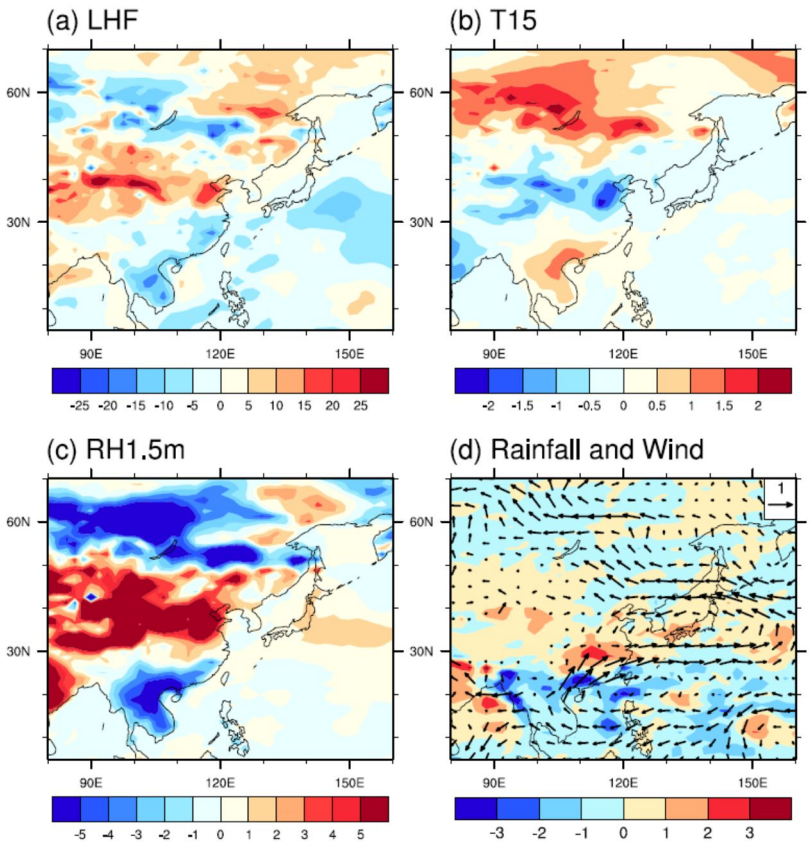

Figure 3.13. Contribution by the land cover changes alone to the future-present differences in summer (represented by (AEnodts – AEnod) – (Ats – A)) in (a) latent heat flux (W m^{-2}), (b) surface air temperature (K), (c) 1.5 m relative humidity (%) and (d) rainfall (shading, mm day^{-1}), 850 hPa wind (vectors, m s^{-1}).

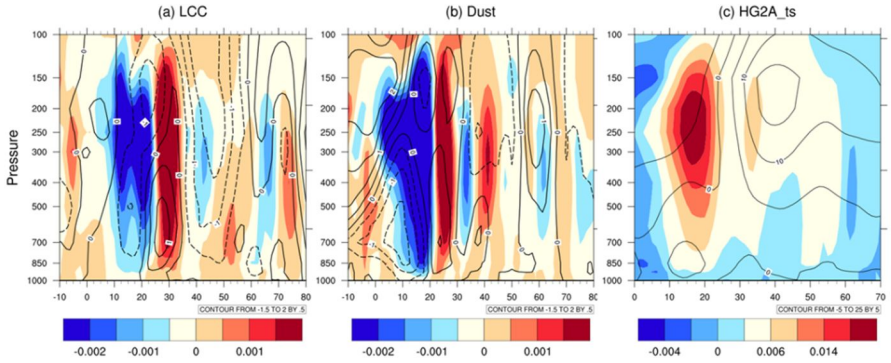

Figure 3.14. (a and b) Contribution to future-present changes in vertical motion (upward: red, downward: blue) and U wind anomalies (solid line: westerlies) from 110-120° E driven by (a) LCC impact, and (b) dust impact. (c) Climatological vertical motion over 110-120° E in the HadGEM2-A timeslice run, Ats.

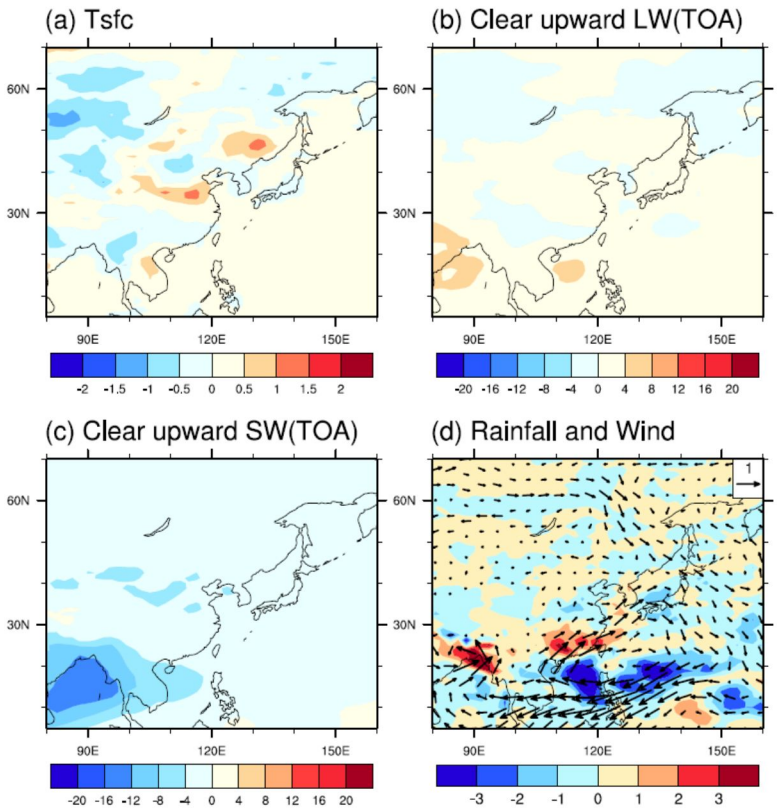

Figure 3.15. As Fig. 3.13 but showing the contribution from the direct radiative effect of dust to the future-present differences in JJA in (a) surface temperature (K), (b) clear sky upward longwave radiation at top of atmosphere (W m^{-2}), (c) clear sky upward shortwave radiation at top of atmosphere (W m^{-2}) and (d) rainfall (shading, mm day^{-1}), 850 hPa wind (vectors, m s^{-1}).

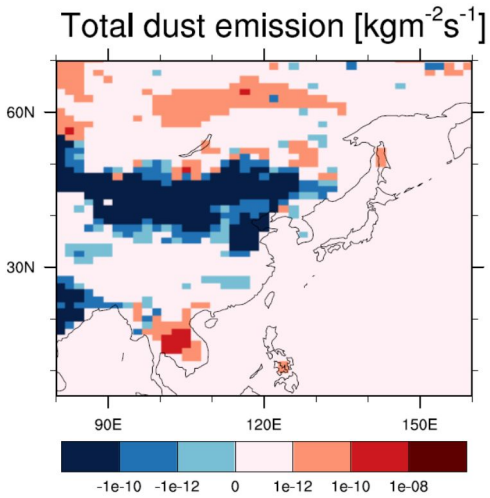

Figure 3.16. Future changes in total dust emission (kg m^{-2} s^{-1}) in JJA from AEts – AE.

3.3.2 Future Experiments

The effect of including a dynamic vegetation model, particularly with the feedback on the dust loading, is expected to affect the simulation of future climate change. Changes in AEts relative to AE show increases in rainfall over SC, KR and the western North Pacific

(Fig. 3.10b). Compared with differences between Ats and A in Fig. 3.10a, Fig. 3.10b shows a further reduction in rainfall over the South China Sea (SCS) to the south of 20°N accompanied by anticyclonic flow at 850hPa. The discrepancy in future changes in precipitation tends to be larger than that of temperature: Fig. 3.10c and 10d present similar warming patterns.

In order to examine the role of different vegetation distributions in global warming, with and without the dust feedbacks, we analyze future timeslice experiments in a similar manner to ML12. To estimate individually the impact of land cover, feedback on the dust loading, and climate change of global warming, we use the experiments described in Table 2. Note that "Dust" and "LCC" are 'double differences' illustrating the impacts of the inclusion of the land cover changes, and the radiative effects of the dust changes that the land cover change induces, on the future-present differences.

According to Baek et al (2013), the warming and rainfall increment from RCP8.5 are expected to be of the order of 6 ±1K and 17% over East Asia. The temperature rises in the timeslice experiments are of similar magnitude (Fig.3. 10c, 10d, 11b). Precipitation is anticipated to increase by 10%-15% toward the end of the twenty-first century over the major monsoonal front region over East Asia in good CMIP5 models simulations under the RCP6.0 scenario (Seo et al., 2013). Consistent with this, Fig. 3.10 and Fig. 3.11 project a warmer and wetter climate in future summer over NC, KR and SC. Fig. 3.10b and Fig. 3.11a show that a larger increase in rainfall between future and present timeslice run is simulated in these regions when land cover change and feedback on the dust are included. However, while precipitation changes over the SCS region tend to be slightly positive on average in climate change-only,

including land cover changes and feedback with dust induces a reduction in rainfall in this region.

The land surface cover differences in this region between future and present-day climate projected by this model are in C_3 grass expansion replacing bare soil (Fig. 3.12c, 12f). These changes contribute increases in the evaporation and latent heat flux and decreases in surface air temperature (Fig. 3.13a, 13b) to the overall future-present changes. Comparison between (AEnodts -AEnod) and (Ats-A) in Fig. 3.10 showed that the changes in land cover contribute to increased rainfall over the land and reduced rainfall over the SCS. Increasing latent heat flux accompanies lower boundary layer height and is associated with boundary layer moistening (Fig. 3.13c). According to Lee et al. (2009, 2011), a more vegetated surface tends to be associated with surface moistening, favoring an increase in latent heat and atmospheric moisture (Fig. 3.13). The changes in vegetation

and associated changes in surface air temperature, latent heat fluxes (Fig. 3.13a,b) and low level circulation (Fig. 3.13d) are in a similar pattern, but opposite sign, to those shown in Fig. 3.6b, 3.7c and 3.9a. This suggests that the future differences between experiments with different land cover (AEnodts - A_ts) are small compared with the present-day differences (AEnod-A) such that the double-difference (AEnodts – AEnod) – (A_ts – A) is dominated by the present-day differences. This is consistent with the findings of ML12.

In Fig. 3.13d, increased rainfall over the SC region from 25°N to 35°N is associated with additional anomalous convergence and upward motion over the SC region (see Fig. 3.14a) induced by the land cover change effect as the monsoon differential circulation results in enhanced moisture transport and cloud formation over SC and KR. Whereas over the SCS, anomalous anticyclonic flow is

related to downward motion from 10°N to 20°N (Fig. 3.14a) and reduced rainfall (Fig. 3.13d).

As shown in Fig. 3.11a, the dust radiative forcing is the main contributor to the reduction of simulated precipitation over SCS to the south of 20°N in the AEts future experiment. Figure 3.15 shows the double-difference (AEts minus AE) minus (AEnodts minus AEnod). The atmospheric response of Fig. 3.15 seems to be largely opposite to that in Fig. 3.9b, 9e and 9f, suggesting that it is dominated by the present-day impacts of dust seen between AE and AEnod. In global warming (i.e. future-present), the bare soil fraction decreases (Fig. 3.12f) so the dust emission of HadGEM2-ES decreases in the future relative to the present climate (Fig. 3.16). As mentioned in Section 3.1.3, the direct radiative effect of dust seems to induce stronger flow than that of ES land cover only effect. The convective region over SC in the future experiment Ats (Fig. 3.10a, 14c) is

strengthened in AEts (Fig. 3.10b), and that over the SCS weakened, through the radiative effects of the reduced dust loading (Fig. 3.14b), with related increases and decreases in precipitation (Fig. 3.15d and 11a).

Overall, for future precipitation projection over East Asia using this model, simulating interactive land cover change by a dynamic vegetation model, and particularly the subsequent changes in dust radiative effect, are at least as important as the warming conditions. In contrast, for future changes in temperature, the global warming effect is dominant among climate change, land cover change and dust radiative effects over East Asia (Fig. 3.10c, 10d and 11b).

Chapter 4. Summary and Conclusion

The primary objective of this study is to investigate the impacts of land surface changes on East Asian climate. This study is mainly composed of two parts; Regional climate response to land surface changes after harvest in the North China Plain under present and possible future climate conditions and the impact of land cover generated by dynamic vegetation model on East Asian climate. Through this study, it was proposed that the biophysical influence of land cover conditions and associated aerosol loading on the rainfall and surface temperature over East Asia.

In section 2, it is evaluated the double-cropping area in the NCP and examined the biophysical effects of land surface type conversion to bare soil during the harvest period. For different GHG emission scenarios, as mentioned in Feddma et al. [2005], Pitman et al. [2011]

and Lawrence et al. [2012], it is necessary to understand the additional response in the surface climate driven by agriculture-related land surface change. Hence, motivated by these previous studies it is evaluated the impacts of harvest-induced land surface change, both under present and possible future climate conditions. It is used HadGEM2-A for the ensemble simulation, and harvest was represented using the monthly varying fraction of vegetation. The results from this study are summarized as follows: (1) The land surface appeared warmer and drier than in surrounding vegetated regions in June after harvest. The simulation results were consistent with the observed values. The conversion of bare soil surface from C3 type vegetation caused biophysical impacts on the surface climate via decreases in evapotranspiration and latent heat flux, which contributed to increases in surface temperature and decreases in surface humidity. (2) The results showed that harvest has the

potential to enhance the warming caused by the GHGs effect by as much as 1.4°C under the minimum RCP 2.6 global warming scenario at the end of the 21st century. This warming effect declined to 1.0°C under the maximum RCP 8.5 scenario because of the projected wetter conditions. The reduced latent heat flux associated with the overall decreases in evapotranspiration contributed to the enhancement of surface warming in possible future.

The effects of land type conversion on regional climate can be mediated by several processes that include changes in albedo that determine the level of solar energy absorption, the partitioning of received energy into latent and sensible heat fluxes, and by changes in surface roughness during the transportation of heat. Among these factors, the contribution of heat fluxes was dominant than albedos or roughness lengths in this study. The warming response simulated in our experiment (Figure 2.5b) was similar to observational

measurements (Figure 2.5a) and the results presented in Ho et al. [2012].

The results from this study suggest the potential impacts from agricultural harvesting practices on local climate not only for present but also for possible future climate. However, the magnitude of the impacts was not proportional to the GHGs induced warming caused by the different climate conditions in each RCP scenario. Nevertheless, our results confirm those of previous studies [Feddema et al., 2005; Pitman and Narisma, 2005; Pitman et al., 2011; Lawrence et al., 2012], which show that on a regional scale, the impact of anthropogenic landscape change on local climate can be comparable to those of GHGs and SSTs in future climate projections.

In section 3, the purpose of this study is assessing the influences of land cover generated by dynamic vegetation model on East Asian climate. The impact of varying land cover distribution, as simulated

by a DGVM, on simulated regional climate over East Asia is examined. The interaction between land cover change by the DGVM and model systematic biases are shown in the present-day climate. The climatology of HadGEM2-A has an underestimation of rainfall over KR in summer and an overestimation over SC. When the land cover from HadGEM2-ES, which uses an interactive vegetation model, is used as an input to HadGEM2-A (experiment AE), the precipitation bias is enhanced over KR and SCS. The difference between AE and A is related to regional bare soil expansion by the DGVM through interaction with the rainfall bias, and also through feedback with the subsequent dust loading, causing a direct radiative effect. The direct radiative effect of dust has an important influence on both the precipitation bias and the stronger circulation response in SLP and wind than the land cover-only effect does. In this study, more dust loading due to excessive bare soil fraction induces an

amplified dry bias over Asia. The land cover difference between AE and A affects the surface air temperature bias. In summer, a warm bias in NC (Fig. 3.7h) is due to bare soil area expansion replacing vegetation (Fig. 3.7). Soil fraction expands (shrinks) and temperature rises (drops) over NC (SC) (Fig. 3.7) through changes in surface roughness, evaporation and latent heat fluxes.

The dust loading is expected to reduce in the future time-slice run, since C3 grass replaces bare soil area over NC. The consequent direct radiative effect of dust changes induces the opposite direction of anomalous wind flow over the SCS compared with that induced by the CO2 increase alone. Thus, in the future projection, suppressed rainfall appears over the SCS. Just as the direct radiative effect is significant in the future precipitation simulation, the land cover effect is also important. The C3 grass expansion replacing bare soil, inducing an increase in latent heat flux, lowers the surface

temperature. The changes in land cover between future and present day tend to oppose the surface warming over NC and KR in summer that are driven by increasing CO2 in the time-slice experiments. When the land cover change impacts and associated dust radiative effect are combined, the resulting rainfall under future climate differs regionally. In contrast with the precipitation response, the temperature response in the time-slice run is dominated by the warming induced from the atmospheric CO2 increase. In terms of the projected temperature rise, the ES land cover and dust radiative effects are very small. Overall, the inclusion of land cover changes as simulated by an interactive vegetation model has impacts on both present and future climate in East Asia. These results are similar to those for India shown in ML12, although the response amplitude is different.

Inclusion of dynamic vegetation components in a climate model allows impacts of climate change on both atmospheric composition and ecosystems. When the various feedbacks among the model components are included, complexity increases and the feedbacks affect more numerous systematic biases in models and future climate projections (ML12). ML12 mentioned that, as Earth System process are included in a model, the systematic biases need to be studied in order to understand how additional feedbacks from the interactive components in Earth system models affect climate projection. Although the details of our results may be dependent on the particular modelling system used for this study, nevertheless they suggest that vegetation feedbacks may be important over East Asia, particularly in the dust emission source regions, for present-day and future climate simulation.

The results from this study suggest the potential impacts from agricultural harvesting practices on local climate not only for present but also for possible future climate. Furthermore, the land cover change feedbacks should be considered over East Asia especially in the dust emission regions both in present-day and future when interpret an Earth System modeling results.

References

Baek, H.-J., J. Lee, H.-S.Lee, C. Cho, W.-T.Kwon, C. Marzin, Y.-K.Hyun, S.-Y.Gan, M.-J.Kim, D.-H.Choi, J. Lee, J. Lee, K.-O. Boo, H.-S. Kang, and Y.-H. Byun (2013), Climate change in the 21st century simulated by HadGEM2-AO under Representative Concentration Pathways, Asia-Pac. J. Atmos. Sci., DOI:10.1007/s13143-013-0053-7

Bayer, L. B., B. J. J. M. van den Hurk, B. J. Strengers, and J. G. van Minnen (2012), Regional feedbacks under changing climate and land-use conditions, Earth Syst. Dynam. Discussions, 3, 201–234, doi:10.5194/esdd-3-201-2012.

Bonan, G. B. (2001), Observational evidence for reduction of daily maximum temperature by croplands in the Midwest United States, J. Clim., 14, 2430–2442, doi:http://dx.doi.org/10.1175/1520-0442(2001)014<2430:OEFROD>2.0.CO;2.

Collins, W. J., N. Bellouin, M. Doutriaux-Boucher, N. Gedney, P. Halloran, T. Hinton, J. Hughes, C. D. Jones, M. Joshi, S. Liddicoat, G. Martin, F. O'Connor, J. Rae, C. Senior, S. Sitch, I. Totterdell, A. Wiltshire, and S. Woodward (2011), Development and evaluation of an Earth-System model – HadGEM2, Geosci. Model Dev., 4, 1051–1075, doi:10.5194/gmd-4-1051-2011.

Cooley, H. S., W. J. Riley, M. S. Tom, and Y. He (2005), Impact of agricultural practice on regional climate in a coupled land surface mesoscale model, J. Geophys. Res., 110, D03113, doi:10.1029/2004jd005160.

Cox, P. M., R. A. Betts, C. B. Bunton, R. L. H. Essery, P. R. Rowntree, and J. Smith (1999), The impact of new land surface physics on the GCM simulation of climate and climate sensitivity, Clim. Dynam., 15, 3, 183–203, doi:10.1007/s003820050276.

Davin, E. L., and N. deNoblet-Ducoudré (2010), Climatic impact of global-scale deforestation: Radiative versus nonradiative processes, J. Clim., 23(1), 97-112, doi:10.1175/2009JCLI3102.1.

De Noblet-Ducoudré, N., J.-P.Boisier, A. Pitman, G. B. Bonan, V. Brovkin, F. Cruz, C. Delire, V. Gayler, B. J. J. M. van den Hurk, P. J. Lawrence, M. K. van der Molen, C. Müller, C. H. Reick, B. J. Strengers, and A. Voldoire (2012), Determining robust impacts of land-use-induced land cover changes on surface climate over North America and Eurasia: Results from the first set of LUCID experiments, J. Clim., 25, 3261–3281, doi:10.1175/JCLI-D-11-00338.1.

Douglas, E. M., D. Niyogi, S. Frolking, J. B. Yeluripati, R. A. Pielke Sr., N. Niyogi, C. J. Vorosmarty, and U. C. Mohanty (2006), Changes in moisture and energy fluxes due to agricultural land use and

irrigation in the Indian Monsoon Belt.Geophys. Res. Lett., 33, *L14403*, doi:10.1029/2006GL026550.

Essery, R. and D. B. Clark (2003), Developments in the MOSES 2 land-surface model for PILPS 2e, Global Planet. Change, 38, 161–164, doi:10.1016/j.bbr.2011.03.031.

Feddema, J. J., K. W. Oleson, G. B. Bonan, L. O. Mearns, L. E. Buja, G. A. Meehl, W. M. Washington (2005), The importance of land-cover change in simulating future climates, Science, 310, 1674–1678, doi:10.1126/science.1118160.

Ge, J. (2010), MODIS observed impacts of intensive agriculture on surface temperature in the southern Great Pains, Int. J. Climatol., 30, 1994–2003, doi:10.1002/joc.2093.

Ho, C.-H., S.-J. Park, S.-J.Jeong, J. Kim, and J.-G Jhun (2012), Observational evidences of double cropping impacts on the

climate in the northern China plains, J. Clim., 25, 4721–4728, doi:10.1175/JCLI-D-11-00224.1.

Hoffmann, W. A. and R. B. Jackson (2000), Vegetation-climate feedbacks in the conversion of tropical savanna to grassland, J. Clim., 13, 1593–1602, doi:http://dx.doi.org/10.1175/1520-0442(2000)013<1593:VCFITC>2.0.CO;2.

Hurtt, G. C., Chini, L. P., Frolking, S., Betts, R., Feddema, J., Fischer,G., Fisk, J. P., Hibbard, K., Houghton, R. A., Janetos, A.,Jones, C., Kindermann, G., Kinoshita, T., Klein Goldewijk, K.,Riahi, K., Shevliakova, E., Smith, S., Stehfest, E., Thomson, A., Thornton, P., van Vuuren, D. P., and Wang, Y. (2011), Harmonization of Land-Use Scenarios for the Period 1500–2100: 600 Years of Global Gridded Annual Land-Use Transitions, Wood Harvest, and Resulting Secondary Lands, Climatic Change, 109, 117–161, doi:10.1007/s10584-011-0153-2, 2011.

Jeong, S.-J., C.-H. Ho, T.-W. Park, J. Kim, and S. Levis (2011), Impact of vegetation feedback on the temperature and its diurnal range over the Northern Hemisphere during summer in a 2XCO_2 climate, Clim. Dynam., 37, 821–833, doi:10.1007/s00382-010-0827-x.

Jones, C. D., J. K. Hughes, N. Bellouin, S. C. Hardiman, G. S. Jones, J. Knight, S. Liddicoat, F. M. O'Connor, R. J. Andres, C. Bell, K.-O. Boo, A. Bozzo, N. Butchart, P. Cadule, K. D. Corbin, M. Doutriaux-Boucher, P. Friedlingstein, J. Gornall, L. Gray, P. R. Halloran, G. Hurtt, W. J. Ingram, J.-F. Lamarque, R. M. Law, M. Meinshausen, S. Osprey, E. J. Palin, L. Parsons Chini, T. Raddatz, M. G. Sanderson (2011), The HadGEM2-ES implementation of CMIP5 centennial simulations. Geosci.Model Dev., 4, 543–570, doi:10.5.5194/gmd-4-543-2011.

Kang, H.-S., D.-H.Cha and D.-K. Lee (2005), Evaluation of the mesoscale model/land surface model (MM5/LSM)coupled model for East Asian summer monsoon simulations, J. Geophys. Res. ,110, D10105, doi:10.1029/2004JD005266.

Kang, H.-S.and S.-Y. Hong (2008), An assessment of the land surface parameters on the simulated regional climate circulations: The 1997 and 1998 east Asian summer monsoon cases, J. Geophys. Res., 113, D15121, doi:10.1029/2007D009499.

Kim, J. and T. Reichler(2011), Regional Performance Skill of Coupled Models in Simulating Present-day Mean Climate, paper presented at the international workshop on Coordinated Regional Climate Downscaling Experiment in East Asia, Korea Meteorological Administration, Jeju, South Korea

Kueppers, L. M. and M. A. Snyder (2012), Influence of irrigated agriculture on diurnal surface energy and water fluxes, surface

climate, and atmospheric circulation in California, Clim. Dynam., 38, 1017–1029.

Lau, K. M., M.-T. Li (1984), The monsoon of East Asia and its global associations-A survey, B. Am. Meteorol. Soc., 65(2)

Lau, K. M., M. K. Kim, and K. M. Kim (2006), Asian monsoon anomalies induced by aerosol direct effects, Clim. Dyn., 26, 855–864, doi:10.1007/s00382-006-0114-z.

Lau, K. M and K.-M. Lau (2006), Observational relationships between aerosol and Asian monsoon rainfall, and circulation, Geophys. Res. Lett., 33, L21810, doi:10.1029/2006GL027546

Lawrence. D. M. and J. M. Slingo (2004), An annual cycle of vegetation in a GCM. Part I: implementation and impact on evaporation, Clim. Dynam., 22, 87–105, doi:10.1007/s00382-003-0366-9.

Lawrence, P. J., J. J. Feddema, G. B. Bonan, G. A. Meehl, B. C. O'Neill, S. Levis, D. M. Lawrence, K. W. Oleson, E. Kluzek, K. Lindsay, and P. E. Thornton (2012), Simulating the biogeochemical and biogeophysical impacts of transient land cover change and wood harvest in the community climate system model (CCSM4) from 1850 to 2100, J. Clim., 25, 3071–3095, doi:10.1175/JCLI-D-11-00256.1.

Lee, E., T. N. Chase, B. Rajagopalan, R. G. Barry, T. W. Biggs, and P. J. Lawrence (2009), Effects of irrigation and vegetation activity on early Indian summer and monsoon variability, Int. J. Climatol., 29, 573–581, doi:10.1002/joc.1721.

Lee, E., C. C. Barford, C. J. Kucharik, B. S. Felzer, and J. A. Foley(2011), Role of turbulent heat fluxes over land in the monsoon over East Asia, Int. J. Geosci., 2, 420–431, doi:10.4236/ijg.2011.24046.

Liu, J., M. Liu, H. Tian, D. Zhuang, Z. Zhang, W. Zhang, X. Tang, and X. Deng (2005), Spatial and temporal patterns of China's cropland during 1990–2000: An analysis based on Landsat TM data, Remote Sensing Environ., 98, 442–456, doi:10.1016/j.rse.2005.08.012.

Lobell, D. B., G. Bala, and P. B. Duffy (2006), Biogeophysical impacts of cropland management changes on climate, Geophys. Res. Lett., 33, L06708, doi:10.1029/2005GL025492.

Loveland, T. R., B. C. Reed, J. F. Brown, D. O. Ohlen, Z. Zhu, L. Yang, and J. W. Merchant (2000), Development of a global land cover characteristics database and IGBP DISCover from 1 km AVHRR data, Int. J. Remote Sensing, 21, 1303–1330, doi:10.1080/014311600210191.

Martin, G. M. and R.C. Levine (2012), The influence of dynamic vegetation on the present-day simulation and future projections

of the South Asian summer monsoon in the HadGEM2 family, Earth Syst. Dynam., 3, 245-261, doi:10.5194/esd-3-245-2012

Moss, R. H., J. A. Edmonds, K. A. Hibbard, M. R. Manning, S. K. Rose, D. P. van Vuuren, T. R. Carter, S. Emori, M. Kainuma, T. Kram, G. A. Meehl, J. F. B. Mitchell, N. Nakicenovic, K. Riahi, S. J. Smith, R. J. Stouffer, A. M. Thomson, J. P. Weyant and T. J. Wilbanks(2010), The next generation of scenarios for climate change research and assessment, Nature, 463, 747-756, doi:10.1038/nature08823.

Nair, U. S., D. K. Ray, J. Wang, S. A. Christopher, T. Lyons, R. M. Welch, and R. A. Pielke Sr., (2007) Observational estimates of radiative forcing due to land use change in southwest Australia. J. Geophys. Res., 112, D09117, doi:10.1029/2006JD007505.

Narisma, G. T. and A. J. Pitman (2003), The impact of 200 years of land cover change on the Australian near-surface climate, J.

Hydrometeorol., 4, 424–436, doi:http://dx.doi.org/10.1175/1525-7541(2003)4<424:TIOYOL>2.0.CO;2.

Osborne, T., J.Slingo, D. Lawrence, and T. Wheeler (2009), Examining the interaction of growing crops with local climate using a coupled crop-climate model, Am. Meteorol. Soc., 22, 1393–1411, doi:10.1175/2008JCLI2494.1.

Piao, S., P. Ciais, Y. Huang, Z. Shen, S. Peng, J. Li, L. Zhou, H. Liu, Y. Ma, Y. Ding, P. Friedlingstein, C. Liu, K. Tan, Y. Yu, T. Zhang, and J. Fang (2010), The impacts of climate change on water resources and agriculture in China, Nature, 467, 43–51, doi:10.1038/nature09364.

Pielke, R. A. and R. Avissar (1990) Influence of landscape structure on local and regional climate. Landscape Ecol., 4, 133–155.

Pielke, R. A. Sr., J. Adegoke, A. Beltran-Przekurat, C. A. Hiemstra, J. Lin, U. S. Nair, D. Niyogi, and T. E. Nobis (2007) An overview of

regional land use and land cover impacts on rainfall. Tellus B, 59, 587–601, doi:10.1111/j.1600-0889.2007.00251.x.

Pielke Sr., R. A., A. Pitman, D. Niyogi, R. Mahmood, C. McAlpine, F. Hossain, K. Goldewijk, U. Nair, R. Betts, S. Fall, M. Reichstein, P. Kabat, and N. de Noblet-Ducoudre (2011) Land use/land cover changes and climate: Modeling analysis and observational evidence, WIREs Clim. Change, 2, 828–850, doi:10.1002/wcc.144.

Pitman, A. J. and G. T. Narsima (2005), The role of land surface processes in regional climate change: a case study of future land cover over south western Australia, Meteorol. Atmos. Phys., 89, 235–249, doi:10.1007/s00703-005-0131-1.

Pitman, A. J., F. B. Avila, G. Abramowitz, Y. P. Wang, S. J. Phipps, and N. de Noblet-Ducoudré (2011), Importance of background climate in determining impact of land-cover change on regional

climate, Nature Clim. Change, 1, 472–475, doi:10.1038/nclimate1294.

Qian Y, D. Gong, J. Fan, L. R. Leung, R. Bennartz, D. Chen and W. Wang (2009), Heavy pollution suppresses light rain in China: Observations and modeling, J. Geophys. Res., 114, D00K02, doi:10.1029/2008JD011575.

Ramanathan, V., C. Chung, D. Kim, T. Betge, L. Buja, J. T. Kiehl, W. M. Washington, Q. Fu, D. R. Sikka, and M. Wild (2005), Atmospheric brown clouds: Impacts on South Asian climate and hydrological cycle, Proc. Natl. Acad. Sci. U. S. A., 102, 5326 – 5333, doi:10.1073/pnas.0500656102.

Ray, D. K., U. S. Nair, R. O. Lawton, R. M. Welch, and R. A. Pielke Sr. (2006), Impact of land use on Costa Rican tropical montane cloud forests: Sensitivity of orographic cloud formation to

deforestation in the plains, J. Geophys. Res., 111, D02108, doi:10.1029/2005JD006096.

Rayner, N. A., E.B. Horton, D.E. Parker, C.K. Folland and R.B. Hackett, September 1996, Version 2.2 of the Global sea-Ice and Sea Surface Temperature data set, 1903-1994, CRTN74, Hadley Centre Meteorological Office, London Road Bracknell Berkshire RG12 2SY

Roy, S. S., R. Mahmood, D. Niyogi, M. Lei, S. A. Foster, K. G. Hubbard, E. Douglas, and R. Pielke Sr. (2007), Impacts of the agricultural green revolution-induced land use changes on air temperatures in India, J. Geophys. Res., 112, D21108, doi:10.1029/2007JD008834.

Reichler, T. and J. Kim (2008), How well do coupled models simulate today's climate, Bull. Am. Meteorol. Soc., 89(3), 303–311, doi:10.1175/BAMS-89-3-303.

Sen, O. L., Y. Wang, and B. Wang (2004), Impact of Indochina deforestation on the East Asian summer monsoon, J. Clim., 17, 1366–1380, doi:http://dx.doi.org/10.1175/1520-0442(2004)017<1366:IOIDOT>2.0.CO;2.

Solomon, S., D. Qin, M. Manning, Z. Chen, M. Marquis, K. B. Averyt, M. Tignor, and H. L. Miller (Eds.) (2007), Contribution of Working Group I to the Fourth Assessment Report of the Intergovernmental Panel on Climate Change, Cambridge University Press, Cambridge, United Kingdom and New York, NY, USA.

Strengers, B. J., C. Müller, M. Schaeffer, R. J. Haarsma,C.Severijns, D. Gerten, S. Schaphoff, R. van den Houdta, and R.Oostenrijka (2010), Assessing 20th century climate-vegetation feedbacks of land-use change and natural vegetation dynamics in a fully

coupled vegetation-climate model, Int. J. Climatol., 30, 2055–2065, doi:10.1002/joc.2132.

Suh M.-S.and D.-K. Lee,Impacts of land use//cover changes on surface climate over east Asiafor extreme climate cases using RegCM2(2004), J. Geophys. Res., 109, D02108, doi:10.1029/2003JD003681.

Takata, K., K. Saito, and T. Yasunari (2009), Changes in the Asian monsoon climate during 1700–1850 induced by preindustrial cultivation, Proc. Natl. Acad. Sci. USA., 106(24), 9586–9589, doi:10.1073/pnas.0807346106.

Taylor, K. E., Stouffer, R. J., and Meehl, G. A (2012), An Overview of CMIP5 and the experiment design, B. Am. Meteorol. Soc., 93, 485–498, doi:10.1175/BAMS-D-11-00094.1.

Xuejie, G., L. Yong, L. Wantao, Z. Zongci, and F. Giorgi (2003), Simulation of effects land use change on climate in China by a

regional climate model, Adv. Atmos. Sci., 20, 583–592, doi:10.1007/BF02915501.

Yamashima, R., K. Takata, J. Matsumoto, and T. Yasunari (2011), Numerical study of the impacts of land use/cover changes between 1700 and 1850 on the seasonal hydroclimate in monsoon Asia, J. Meteorol. Soc. Japan, 89A, 291–298, doi:10.2151/jmsj.2011-A19.

Yoshioka, M., N. M. Mahowald, A. J. Conley, W. D. Collins, D. W. Fillmore, C. S. Zender and D. B. Coleman (2007), Impact of desert dust radiative forcing on Sahel precipitation: relative importance of dust compared to sea surface temperature variations, vegetation changes, and greenhouse gas warming, J. Clim., 20, 1445-1467, DOI: 10.1175/JCLI4056.1.

국문 초록

전구 평균된 토지피복의 변화에 의한 복사강제력은 약 -0.2±0.2 Wm^{-2} 로 작게 나타나지만, 역사적으로 큰 토지이용 및 토지피복의 변화를 겪은 동아시아 지역에서는 그 영향이 온실기체나 해수면온도의 크기에 상응한다고 알려져 있다. 기후변화를 보다 잘 이해하기 위해서 농경지의 확장과 관련된 토지피복의 변화에 대해 많은 연구가 수행되었다. 하지만 동아시아 지역에 대해 농지 면적의 확대를 고려하지 않고 정해진 농지 면적 내에서 토지 이용의 변화가 주는 기후학적 영향을 현재 및 미래에 대해 평가한 연구는 거의 없다. 또한, 동아시아에 대해 토지 피복의 변화가 동반하는 먼지 에어로솔과 토지 피복의 영향을 동시에 고려한 연구 또한 거의 없다. 따라서 본 연구에서는 이모작 지역에서 수확 후에 발생하는 토지이용의 변화 및 동적식생모델이 생산한 토지피복이 동아시아 지역 기후에 주는 영향을 조사하였다.

농경지 이용과 관련한 연구에서는 중국 화북 평원의 이모작 지역에서 수확 후에 발생하는 지면의 변화가 지역 기후에 주는 영향을 조사하였다. 관측 및 모델 연구를 통해 수확 후에 지면이 건조해지고 기온이 상승함을 보였다. 겨울 밀을 수확한 후인 6 월에 지표가 나지로 드러남에 따라서 지표에서 대기로의 증발산이 감소함에 따라서 잠열속이 감소하여 지면 근처가 건조하고 온난해지는 것으로 분석되었다.

대표농도경로 2.6 과 8.5 두 가지 시나리오를 이용한 미래전망 실험에서, 온실기체가 이끄는 온난화에 수확으로 인해 온난화가 가중될 것으로 전망되었다.

한편, 동적식생모델이 생산한 토지 피복과 관련해서 동아시아 지역에 대한 토지피복의 변화와 이것이 동반하는 먼지 에어로솔이 동아시아 지역의 여름철 기온 및 강수 모의에 미치는 영향을 조사하였다. 본 연구에서 사용한 기후모델은 한국과 남중국해 주변에 강수를 적게 모의하는 오차를 가지고 있었다. 이 기후모델과 동적식생모델을 결합시켜 모의되는 지면피복의 변화는 동북아시아의 먼지(황사) 배출 지역에 직접 복사 효과를 수반하였다. 이러한 먼지의 직접복사효과는 강수의 오차를 증가시키는 반면, 지면피복의 물리적 변화는 북중국과 같이 온난 오차를 가지고 있는 지역의 오차를 증가시키는 경향이 있었다. 미래에 대한 전망에 있어서 먼지 배출이 감소하며 남중국해에 고기압성 순환이 증가하면서 강수를 감소시키고 한국과 남중국에는 강수를 증가시켰다. 이러한 강수의 변화와는 반대로, 기온의 전망에 대해서는 온실기체인 이산화탄소의 영향이 지배적인 것으로 나타나 지면피복의 물리적 효과 및 간접영향인 먼지의 직접복사효과는 매우 작은 영향을 주었다.

본 논문에서는 동아시아 지역에 대해 모델링 연구를 통해 현재뿐 아니라 가능한 미래에 수확 후 지표변화가 지역 기후 모의에

주는 영향을 최초로 평가하였으며, 지면피복 및 이와 관련된 먼지의 직접복사효과가 지역의 기온 및 강수의 모의에 주는 영향을 동시에 최초로 평가하였다.

주요어: 토지 이용 지면 피복 변화, 동아시아, 기후 모의, 화북평원, 먼지복사효과, 지구시스템모델

학번: 2003-30139